



Search for dark matter in events with energetic, hadronically decaying top quarks and missing transverse momentum at $\sqrt{s} = 13$ TeV

The CMS Collaboration*

Abstract

A search for dark matter is conducted in events with large missing transverse momentum and a hadronically decaying, Lorentz-boosted top quark. This study is performed using proton-proton collisions at a center-of-mass energy of 13 TeV, in data recorded by the CMS detector in 2016 at the LHC, corresponding to an integrated luminosity of 36 fb^{-1} . New substructure techniques, including the novel use of energy correlation functions, are utilized to identify the decay products of the top quark. With no significant deviations observed from predictions of the standard model, limits are placed on the production of new heavy bosons coupling to dark matter particles. For a scenario with purely vector-like or purely axial-vector-like flavor changing neutral currents, mediator masses between 0.20 and 1.75 TeV are excluded at 95% confidence level, given a sufficiently small dark matter mass. Scalar resonances decaying into a top quark and a dark matter fermion are excluded for masses below 3.4 TeV, assuming a dark matter mass of 100 GeV.

Published in the Journal of High Energy Physics as doi:10.1007/JHEP06(2018)027.

1 Introduction

The existence of dark matter (DM) can be inferred through astrophysical observations of its gravitational interactions [1–3]. The nature of DM has remained elusive, although it is widely believed that it may have a particle physics origin. Multiple models of new physics predict the existence of weakly interacting, neutral, massive particles that provide excellent sources of DM candidates. Searches for DM are often carried out through direct searches for interactions between cosmic DM particles and detectors (e.g., via nuclear recoil [4]), or for particles produced in the annihilation or decay of relic DM particles [5]. The CERN LHC presents a unique opportunity to produce DM particles as well as study them. In this paper, we describe a search for events where DM particles are produced in association with a top quark (hereafter called “monotop”), originally proposed in Ref. [6]. The associated production of a top quark and invisible particles is heavily suppressed in the standard model (SM). Therefore, this signature can be used to probe the production of DM particles via a flavor-violating mechanism, which most DM models do not consider [2]. Searches for the monotop final state have been carried out by the CDF experiment [7] at the Fermilab Tevatron, and by the CMS [8] and ATLAS [9] experiments at the CERN LHC at $\sqrt{s} = 8$ TeV. The present search utilizes 13 TeV data accumulated by the CMS experiment in 2016, corresponding to an integrated luminosity of 36 fb^{-1} . To improve the sensitivity of the analysis compared to previous work, we employ new techniques for the reconstruction and identification of highly Lorentz-boosted top quarks.

In this search, we consider events with a top quark that decays to a bottom quark and a W boson, where the W boson decays to two light quarks. The three quarks evolve into jets of hadrons. This decay channel has the largest branching fraction (67%) and is fully reconstructable. Jets from highly Lorentz-boosted top quarks are distinguished from other types of hadronic signatures by means of a novel jet substructure discriminant, described in Section 3.

We interpret the results in terms of two monotop production mechanisms, example Feynman diagrams for which are shown in Fig. 1. One model involves a flavor-changing neutral current (FCNC), where a top quark is produced in association with a vector boson that has flavor-changing couplings to quarks and can decay to a pair of DM particles. This is referred to in this paper as the “nonresonant” mode. In a simplified model approach, the interaction terms of the effective Lagrangian [6, 10, 11] describing nonresonant monotop production are given by:

$$\mathcal{L}_{\text{int}} = V_\mu \bar{\chi} \gamma^\mu (g_\chi^V + g_\chi^A \gamma_5) \chi + \bar{q}_u \gamma^\mu (g_u^V + g_u^A \gamma_5) q_u V_\mu + \bar{q}_d \gamma^\mu (g_d^V + g_d^A \gamma_5) q_d V_\mu + \text{h.c.}, \quad (1)$$

where “h.c.” refers to the Hermitian conjugate of the preceding terms in the Lagrangian. The heavy mediator is denoted V , and χ is the DM particle, assumed to be a Dirac fermion. The couplings g_χ^V and g_χ^A are respectively the vector- and axial vector-couplings between χ and V . In the quark- V interaction terms, it is understood that q_u and q_d represent three generations of up- and down-type quarks, respectively. Correspondingly, g_u^V and g_u^A are 3×3 flavor matrices that determine the vector- and axial vector-couplings between V and u , c , and top quarks. It is through the off-diagonal elements of these matrices that monotop production becomes possible. To preserve $SU(2)_L$ symmetry, analogous down-type couplings g_d^V and g_d^A must be introduced, and the following must be satisfied [6]:

$$g_u^V - g_u^A = g_d^V - g_d^A. \quad (2)$$

By choice, we assume $g_u^V = g_d^V \equiv g_q^V$, and $g_u^A = g_d^A \equiv g_q^A$, both satisfying the above constraint. Moreover, to focus specifically on monotop production, the only nonzero elements of g_q^V and g_q^A are assumed to be those between the first and third generations.

The second model contains a colored, charged scalar ϕ that decays to a top quark and a DM fermion ψ [11]. In this “resonant” model the interaction terms of the effective Lagrangian are given by:

$$\mathcal{L}_{\text{int}} = \phi \bar{d}_i^C [(a_q)^{ij} + (b_q)^{ij} \gamma^5] d_j + \phi \bar{t} [a_\psi + b_\psi \gamma^5] \psi + \text{h.c.} \quad (3)$$

The Lagrangian includes interactions between the scalar resonance ϕ and down-type quarks d_i , controlled by the couplings a_q (scalar) and b_q (pseudoscalar). Similarly, the couplings a_ψ and b_ψ allow for the decay of ϕ to a top quark and a DM fermion ψ . We assume $a_q = b_q = 0.1$ and $a_\psi = b_\psi = 0.2$. A detailed motivation of these conventions is given in Ref. [11]. Signal model kinematic distributions are presented in Figures A.1-A.2 in Appendix A.

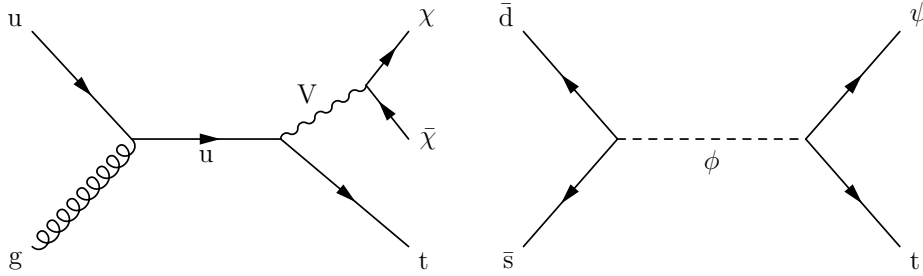


Figure 1: Example Feynman diagrams of monotop production via a flavor-changing neutral current V (left) and a charged, heavy scalar resonance ϕ (right).

2 The CMS detector, particle reconstruction, and event simulation

The CMS detector, described in detail in Ref. [12], is a multipurpose apparatus designed to study high-transverse momentum (p_T) processes in proton-proton and heavy-ion collisions. A superconducting solenoid occupies its central region, providing a magnetic field of 3.8 T parallel to the beam direction. Charged particle trajectories are measured using silicon pixel and strip trackers that cover a pseudorapidity region of $|\eta| < 2.5$. A lead tungstate (PbWO_4) crystal electromagnetic calorimeter (ECAL) and a brass and scintillator hadron calorimeter (HCAL) surround the tracking volume and extend to $|\eta| < 3$. The steel and quartz-fiber forward Cherenkov hadron calorimeter extends the coverage to $|\eta| < 5$. The muon system consists of gas-ionization detectors embedded in the steel flux-return yoke outside the solenoid and covers $|\eta| < 2.4$. The return yoke carries a 2 T return field from the solenoid. The first level of the CMS trigger system is designed to select events in less than $4 \mu\text{s}$, using information from the calorimeters and muon detectors. The high-level trigger-processor farm reduces the event rate to several hundred Hz.

The particle-flow (PF) event algorithm [13] reconstructs and identifies each individual particle through an optimized combination of information from the different elements of the CMS detector. The energy of a photon is obtained directly from the ECAL measurement, corrected for effects from neglecting signals close to the detector noise level (often termed zero-suppression). The energy of an electron is determined from a combination of the electron momentum at the primary interaction vertex as determined by the tracker, the energy of the corresponding ECAL cluster, and the energy sum of all photons spatially compatible with originating from the electron track. The energy of a muon is obtained from the curvature of the corresponding track. The energy of a charged hadron is determined from a combination of its momentum measured in the tracker and the matching ECAL and HCAL energy deposits, corrected for zero-suppression effects and for the response function of the calorimeters to hadronic showers.

Finally, the energy of a neutral hadron is obtained from the corresponding corrected ECAL and HCAL energy.

The DM signal is generated by Monte Carlo (MC) simulation using MADGRAPH5_aMC@NLO v2.4.3 [14]. Events for the nonresonant production are calculated at next-to-leading order (NLO) in quantum chromodynamics (QCD) perturbation theory. Masses for the mediator V of $m_V > 200 \text{ GeV}$ are considered in order to provide an SM-like top quark width, i.e., to avoid decays of the top quark into a u quark plus an on-shell (for $m_V < m_t$) or off-shell (for $m_t \approx m_V - \Gamma_V$) mediator V , where Γ_V is the width of V . The resonant mode is generated at leading order (LO) accuracy.

To model the expectations from SM backgrounds, the $t\bar{t}$ and single top quark backgrounds are generated at NLO in QCD using POWHEG v2 [15–17]. Predictions for ZZ , WZ , or WW (i.e., diboson) production are obtained at LO with PYTHIA 8.205 [18]. Events with multiple jets produced through the strong interaction (referred to as QCD multijet events) are simulated at LO using MADGRAPH5_aMC@NLO v2.3.3. Simulated samples of Z +jets, W +jets, and γ +jets processes are generated at LO using MADGRAPH5_aMC@NLO v2.3.3, which matches jets from the matrix element calculations to parton shower jets using the MLM prescription [19]. The samples are corrected by weighting the p_T of the respective boson with NLO QCD K-factors obtained from large samples of events generated with MADGRAPH5_aMC@NLO and the FxFx merging technique [20]. The samples are further corrected by applying NLO electroweak K-factors obtained from calculations [21–23] that depend on boson p_T .

All samples produced using MADGRAPH5_aMC@NLO or POWHEG are interfaced with PYTHIA 8.212 for parton showering, hadronization, and fragmentation, using the CUETP8M1 [24, 25] underlying-event tune. The appropriate LO or NLO NNPDF3.0 sets [26] are used for the parametrization of the parton distribution functions (PDF) required in all these simulations. The propagation of all final state particles through the CMS detector are simulated with GEANT4 [27]. To model the impact of particles from additional proton-proton interactions in an event (pileup), the number of simulated interactions is adjusted to match the distribution observed in the data [28].

3 Hadronically decaying top quark identification

For top quark $p_T > 250 \text{ GeV}$, the decay products are expected to be contained within a distance of $\Delta R = 1.5$ relative to the top quark, where $\Delta R = \sqrt{(\Delta\eta)^2 + (\Delta\phi)^2}$, and $\Delta\eta$ and $\Delta\phi$ are, respectively, the differences in pseudorapidities and azimuthal angles, where $\Delta\phi$ is measured in radians. The final state particles of the hadronization of a light quark or gluon are reconstructed as a jet. A standard jet-clustering algorithm at CMS is the anti- k_T algorithm [29] with a distance parameter of 0.4 (AK4). If a hadronically decaying top quark is highly Lorentz-boosted, reconstructing the three daughter quarks separately becomes difficult, as the resulting jets tend to overlap in the detector. Accordingly, to identify such signatures, we define CA15 jets as objects that are clustered from PF candidates using the Cambridge–Aachen algorithm [30] with a distance parameter of 1.5. To reduce the impact of particles arising from pileup, weights calculated with the pileup per particle identification (PUPPI) algorithm [31] are applied to the PF candidates. Calibrations derived from data are then applied to correct the absolute scale of the jet energy [32]. The CA15 jets must pass the selection criteria $p_T > 250 \text{ GeV}$ and $|\eta| < 2.4$. To be identified as arising from top quark decays, jets must have a mass within a specified interval containing the top quark mass, have a high likelihood of containing a bottom quark, and exhibit certain substructure characteristics. Such jets are referred to as “t-tagged” jets hereafter.

The ‘‘soft drop’’ (SD) [33] grooming method is used to remove soft and wide-angle radiation produced within jets through initial state radiation or through the underlying event. Removing such radiation, the SD algorithm defines a subset of the CA15 jet’s constituents, which are further grouped into subjets of the CA15 jet. The grooming is done using the SD parameters $z_{\text{cut}} = 0.15$ and $\beta = 1$ (for their definition, see Ref. [33]), chosen to optimize the resolution in the mass of the groomed jet m_{SD} . Hereafter, when the SD algorithm is referred to, these parameters are used. We require t -tagged jets to satisfy $110 < m_{\text{SD}} < 210$ GeV to be compatible with the expectations of a top quark.

To identify the b quark in the CA15 jet expected from a top quark decay, we use the combined secondary vertex (CSVv2) algorithm [34, 35]. The b tagging criterion is then defined by requiring at least one subjet to have a CSVv2 score higher than a specified threshold. The chosen threshold corresponds to correctly identifying a bottom jet with a probability of 80%, and misidentifying a light-flavor jet with a probability of 10%.

3.1 Substructure

Three classes of substructure observables are employed to distinguish top quark jets from the hadronization products of single light quarks or gluons (hereafter referred to as ‘‘ q/g jets’’). These observables serve as inputs to a boosted decision tree (BDT) [36], which is used as the final discriminator.

The N -subjettiness variable (τ_N) [37] tests the compatibility of a jet with the hypothesis that it is composed of N prongs. For top quark decays, a three-pronged topology is expected, while q/g jets may have fewer prongs. This makes the ratio τ_3/τ_2 a robust variable for top quark identification. In this study, the N -subjettiness is computed after jet constituents have been removed using SD grooming, which reduces the p_T - and mass-dependence of τ_3/τ_2 .

The HEPTOPTAGGERV2 uses the mass drop and filtering algorithms [38] to construct subjets within the CA15 jet. The algorithm then chooses the three subjets that are most compatible with top quark decay kinematics. The HEPTOPTAGGERV2 defines a discriminating variable f_{rec} , which quantifies the difference between the reconstructed W boson and top quark masses and their expected values:

$$f_{\text{rec}} = \min_{i,j} \left| \frac{m_{ij}/m_{123}}{m_W/m_t} - 1 \right|, \quad (4)$$

where i, j range over the three chosen subjets, m_{ij} is the mass of subjets i and j , and m_{123} is the mass of all three subjets.

Finally, energy correlation functions (ECF) $a e_N^{(\alpha)}$ are considered, which are sensitive to correlations among the constituents of the jet [39, 40]. They are N -point correlation functions of the constituents’ momenta, weighted by the angular separation of the constituents in η and ϕ . For a jet containing N_p particles, an ECF is defined as

$$a e_N^{(\alpha)} = \sum_{1 \leq i_1 < i_2 < \dots < i_N \leq N_p} \left[\prod_{1 \leq k \leq N} \frac{p_T^{i_k}}{p_T^J} \right] \prod_{m=1}^a \left[\min^{(m)} \left\{ \Delta R_{i_j, i_k} \mid 1 \leq j < k \leq N \right\} \right]^\alpha, \quad (5)$$

where i_1, \dots, i_N range over the jet constituents. The symbols p_T^J and $p_T^{i_k}$ are, respectively, the p_T of the jet and the constituent i_k . The notation $\min^{(m)} X$ refers to the m th smallest element of the set X . We denote the distance ΔR between constituents i_j and i_k as $\Delta R_{i_j, i_k}$. The parameters N and a must be positive integers, and α must be positive.

Discriminating substructure variables are constructed using ratios of these functions:

$$\frac{a e_N^{(\alpha)}}{\left(b e_M^{(\beta)}\right)^x}, \text{ where } M \leq N \text{ and } x = \frac{a\alpha}{b\beta}. \quad (6)$$

In Eq. (6), the six adjustable parameters are N , a , α , M , b , and β . The value of x is chosen to make the ratio dimensionless. As with N -subjettiness, SD grooming is applied to the jet prior to computing the ECFs.

The following 11 ratios of ECFs are found useful for discriminating top quark jets from q/g jets:

$$\begin{aligned} & \frac{1e_2^{(2)}}{\left({}_1e_2^{(1)}\right)^2}, \frac{1e_3^{(4)}}{2e_3^{(2)}}, \frac{3e_3^{(1)}}{\left({}_1e_3^{(4)}\right)^{3/4}}, \frac{3e_3^{(1)}}{\left({}_2e_3^{(2)}\right)^{3/4}}, \frac{3e_3^{(2)}}{\left({}_3e_3^{(4)}\right)^{1/2}}, \\ & \frac{1e_4^{(4)}}{\left({}_1e_3^{(2)}\right)^2}, \frac{1e_4^{(2)}}{\left({}_1e_3^{(1)}\right)^2}, \frac{2e_4^{(1/2)}}{\left({}_1e_3^{(1/2)}\right)^2}, \frac{2e_4^{(1)}}{\left({}_1e_3^{(1)}\right)^2}, \frac{2e_4^{(1)}}{\left({}_2e_3^{(1/2)}\right)^2}, \frac{2e_4^{(2)}}{\left({}_1e_3^{(2)}\right)^2}. \end{aligned} \quad (7)$$

The final tagger is constructed by training a BDT using these thirteen variables (τ_3/τ_2 , f_{rec} , and the ECF ratios) as inputs. Figure 2 shows the BDT response and its performance in discriminating top quark jets from q/g jets. At 50% signal efficiency, the BDT background acceptance is 4.7%, compared to 6.9% for groomed τ_3/τ_2 , which is commonly used for t tagging. The distributions in BDT output and m_{SD} in MC and data are shown in Fig. 3, using control data enriched either in genuine top quark jets from $t\bar{t}$ production or in q/g jets. The selection of these control data is described in Section 5.1. In all distributions, a slight disagreement between data and simulation is observed. This is accounted for by the use of data-driven estimates and scale factors, as described in Section 5.

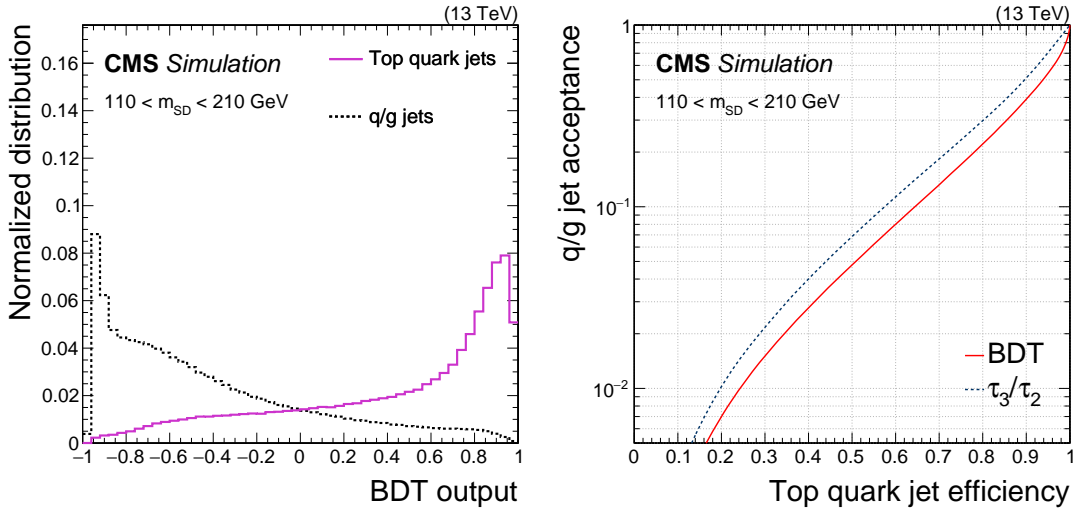


Figure 2: Performance of BDT tagging of top quark and q/g jets. The left figure shows the BDT output in both types of jets. The right figure shows the rate of misidentifying a q/g jet as a function of the efficiency of selecting top jets. In both figures, the p_{T} spectra of jets are weighted to be uniform, and the m_{SD} is required to be in the range of 110–210 GeV.

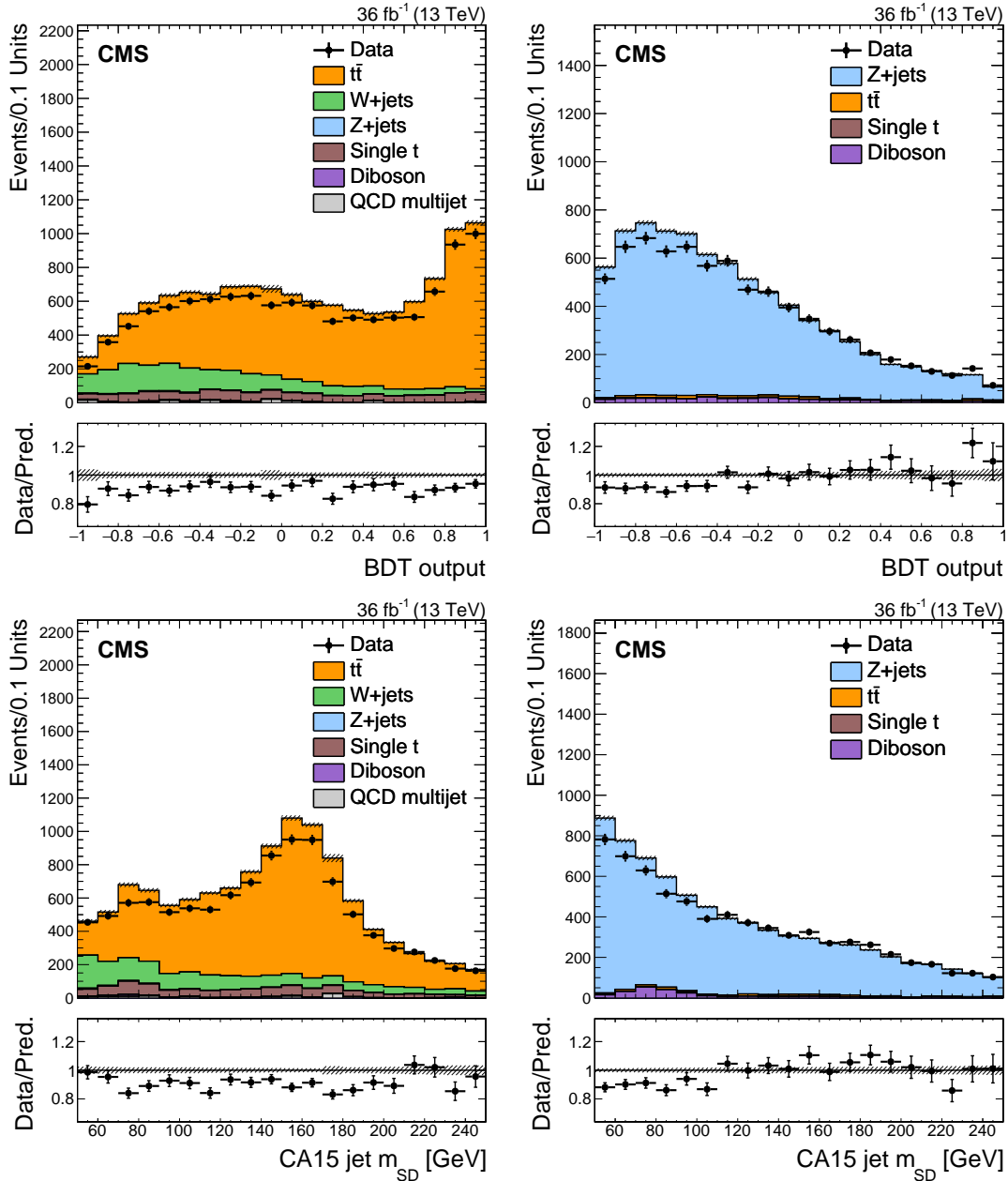


Figure 3: Comparison of the BDT response (upper) and m_{SD} (lower) in data and in simulation, in samples enriched in top-quark jets (left) and q/g jets (right). The lower panel of each plot shows the ratio of the observed data to the SM prediction in each bin. The shaded bands represent the statistical uncertainties in the simulation.

4 Event selection

4.1 Signal topology selection

To search for monotop production, events are selected with two characteristic signatures: a large missing transverse momentum arising from DM candidates and a high- p_T CA15 jet from the decay of a top quark. Events in the signal region (SR) are selected by a logical “or” of triggers with different minimum thresholds (90, 100, 110, or 120 GeV) for both $p_{T,\text{trig}}^{\text{miss}}$ and $H_{T,\text{trig}}^{\text{miss}}$. In the trigger, $p_{T,\text{trig}}^{\text{miss}}$ is defined by the magnitude of the vectorial p_T sum of all PF particles at the trigger level, and $H_{T,\text{trig}}^{\text{miss}}$ by the magnitude of the similar sum of all AK4 jets with $p_T > 20$ GeV and $|\eta| < 5.2$. Muons are not included in these calculations. Additional requirements are imposed on the energy depositions of the jets used to compute $H_{T,\text{trig}}^{\text{miss}}$ to remove events resulting from instrumental effects.

In addition to CA15 jets, this search also utilizes jets clustered using the AK4 algorithm. These will hereafter be referred to as “AK4 jets” and must have $p_T > 30$ GeV and satisfy $|\eta| < 4.7$. The momenta of AK4 jets are corrected to account for mismeasurement of jet energy and for discrepancies between data and simulation [32].

The main observable in this analysis is p_T^{miss} , defined as the magnitude of the sum \vec{p}_T^{miss} of p_T vectors of all final state particles reconstructed using the PF algorithm. Corrections to the momenta of AK4 jets reconstructed in the event are propagated to the p_T^{miss} calculation. A selected event is required to have $p_T^{\text{miss}} > 250$ GeV. The contribution from events with a large misreconstructed p_T^{miss} value is reduced by removing events with beam halo particles, noise, or misreconstructed tracks. For events passing the analysis selection, the efficiency of the triggers is found to be greater than 99%.

To search for events with one hadronically decaying top quark and large p_T^{miss} , we require the presence of exactly one CA15 jet in the event. The CA15 jet must pass the mass and b tagging requirements described in Section 3. To account for discrepancies in b tagging between data and simulation, additional corrections are applied to simulated events. The BDT described in Section 3 is used to split the SR into two categories. In the less restricted or “loose” category, the CA15 jet is required to have a BDT score greater than 0.1 and less than 0.45, while the “tight” category requires a minimum BDT score of 0.45. These values were chosen to optimize the sensitivity of the search.

4.2 Background rejection

Monotop events with hadronically decaying top quarks are characterized by the signatures described in Section 4.1. Several SM processes can mimic these characteristics. Events involving pair production of top quarks, in which one top quark decays to $\ell\nu b$ and the other to $q\bar{q}'b$, can have large p_T^{miss} and a CA15 jet. Likewise, events with $W \rightarrow \ell\nu$ and $Z \rightarrow \nu\nu$ can be characterized by large p_T^{miss} , and jets produced in association with the vector bosons can pass the t tagging selection.

To suppress these and other backgrounds, events are vetoed if they contain at least one well-identified and isolated electron, muon, tau lepton, or photon, passing the criteria described in the following paragraphs.

An electron or muon must have $p_T > 10$ GeV. In the case of electrons, additional criteria are imposed on the ECAL energy deposition, based on the distribution of energy in the shower and the presence of a nearby track [41]. To define an isolated electron, we compute the sum of the energies of the PF particles (charged and neutral hadrons and photons) within a cone of

$\Delta R < 0.3$ around the electron direction. If this sum is less than 17.5% (15.9%) of the electron energy for electrons with $|\eta| < 1.479$ ($1.479 < |\eta| < 2.5$), the electron is considered isolated. In the case of muons, a track must be consistent with the energy depositions in the muon detectors. An isolated muon is defined by setting an energy fraction ceiling of 20% in a cone of $\Delta R < 0.4$. The tau leptons that decay to hadrons plus ν_τ are required to have $p_T > 18$ GeV and are identified from jets that contain a subset of particles with a mass consistent with the decay products of a hadronically decaying tau lepton. An additional set of identification and isolation criteria is applied to tau lepton candidates [13]. Photons must have $p_T > 15$ GeV and satisfy criteria on the distribution of energy depositions in the ECAL, to distinguish them from electrons or jets. Furthermore, to avoid misidentifying an electron as a photon, the ECAL deposition of a photon candidate must not be near a track.

We define an isolated jet to be an AK4 jet that has $\Delta R > 1.5$ relative to the CA15 jet. Since isolated jets are only used to identify b jets, an isolated jet is further required to satisfy $|\eta| < 2.4$ and to lie within the tracker acceptance. To reduce the $t\bar{t}$ background, an event is rejected if there is an isolated jet that is likely to arise from the hadronization of a bottom quark. The b jets are identified using the same CSVv2 algorithm and working point used to identify b quarks inside a CA15 jet. As in the case of tagging CA15 jets, simulated events are corrected for discrepancies in the modeling of isolated jet b tagging. To reduce the background from QCD multijet events in which large p_T^{miss} arises from the mismeasurement of jet momenta, the minimum azimuthal angle between the \vec{p}_T^{miss} direction and any AK4 jet has to be larger than 0.5 rad.

5 Signal estimation

A fit to the p_T^{miss} distribution in the SR is performed to search for the DM signal. After applying the selection described in Section 4, the dominant predicted backgrounds are $t\bar{t}$, $Z(\nu\nu)$ +jets, and $W(\ell\nu)$ +jets. The contributions from these SM processes are estimated using constraints from a simultaneous fit of seven control regions (CR), to be introduced in Section 5.1. The CRs are designed to target dimuon, dielectron, single-photon, single-muon, or single-electron events, with requirements on the substructure and the mass of the CA15 jet that are the same as in the SR.

In the CRs, the distribution of the backgrounds in p_T of recoiling jets (p_T^{recoil}) is used to model the p_T^{miss} distribution in the SRs. The recoil p_T^{recoil} is defined by removing leptons or photons (depending on the CR) from the p_T^{miss} calculation. The primary backgrounds in the SR are constrained by defining transfer factors from the CRs to the SR in bins of p_T^{recoil} . Additional information on the transfer factors and their theoretical and experimental uncertainties is given in Sections 5.2 and 5.3. Each CR is split into loose and tight categories, using the same BDT criteria as the SR categories. Each loose (tight) CR is used to constrain the target background only in the loose (tight) category of the SR. Single top quark, diboson, and QCD multijet backgrounds are not constrained by the CR fit and are estimated using MC simulation.

A binned likelihood fit is performed simultaneously to the p_T^{recoil} distributions in all signal and control regions. The predictions from the CRs are translated to the SR through transfer factors that correlate corresponding bins across all regions. These transfer factors can vary within their uncertainties, as described in Section 5.3.

5.1 Control regions

To estimate the contribution from $Z(\nu\nu)$ +jets in the SR, we use CRs enriched in dimuon, dielectron, and photon events.

Dimuon events are selected employing the same $p_{T,\text{trig}}^{\text{miss}}$ triggers used in the SR, since these triggers do not include muons in the $p_{T,\text{trig}}^{\text{miss}}$ calculation. Events are required to have two well-identified oppositely charged muons that form an invariant mass between 60 and 120 GeV. At least one of the two muons must have $p_T > 20$ GeV and pass tight identification and isolation requirements. Events in the dimuon region must also pass almost all of the other selection requirements imposed on the events in the SR, wherein p_T^{recoil} is substituted for p_T^{miss} . To increase the number of events in the dimuon CR, the requirement for having a CA15 jet b tag is not imposed.

Dielectron events are selected using single-electron triggers, which have a p_T threshold of 27 GeV. Two well-identified oppositely charged electrons are required, and they must form an invariant mass between 60 and 120 GeV. To reach plateau efficiency with respect to the electron p_T , at least one of the two electrons must have $p_T > 40$ GeV and satisfy tight identification and isolation requirements. All selection criteria applied in the dimuon CR are also applied in the dielectron CR.

The γ +jets control sample is constructed using events with at least one high- p_T photon. A single-photon trigger with a p_T threshold of 165 GeV is used to record these events. The event selection requires the photon to have a p_T greater than 175 GeV in order to ensure that the trigger is fully efficient. The photon candidate is required to pass identification and isolation criteria, and must be reconstructed in the ECAL barrel ($|\eta| < 1.44$) to obtain a purity of 95% [42]. As in the dilepton regions, the CA15 jet b tag requirement is not applied in the photon region.

Background events can enter the signal selection because of the loss of a single lepton, primarily from $W(\ell\nu)$ +jets and lepton+jets $t\bar{t}$ events. To estimate these backgrounds, four single lepton control samples are used, defined by selecting electrons or muons and by requiring or vetoing b-tagged jets. The b-tagged single lepton CRs are enhanced in $t\bar{t}$ events, while the b-vetoed single lepton CRs target $W(\ell\nu)$ +jets events.

Single-muon events are selected using the $p_{T,\text{trig}}^{\text{miss}}$ trigger. The muon candidate in these events is required to have $p_T > 20$ GeV, and pass tight identification and isolation requirements. With the exception of b tagging, all other selection requirements used for signal events are imposed, using p_T^{recoil} instead of p_T^{miss} . In addition, to suppress QCD multijet events in which a jet passes the muon identification criteria and the p_T^{miss} is mismeasured, the transverse mass (m_T) is required to be less than 160 GeV, where $m_T = \sqrt{2p_T^{\text{miss}}p_T^\ell(1 - \cos \Delta\phi(\vec{p}_T^{\text{miss}}, \vec{p}_T^\ell))}$. In the b-tagged single-muon CR, we require the CA15 jet to be b-tagged as in the SR, and we further require exactly one b-tagged isolated jet. In the b-vetoed single-muon CR, the b tagging requirements are reversed, so that the CA15 jet is not b-tagged and there are no b-tagged isolated jets.

The single-electron CRs are defined in a fashion similar to the single-muon CRs. Events are selected using the single-electron trigger, and the p_T of the electron is required to be greater than 40 GeV. An additional requirement of $p_T^{\text{miss}} > 50$ GeV is imposed on single-electron events to suppress the multijet background.

A summary of the selection criteria for the SR and for all of the CRs is given in Table 1.

To account for discrepancies between data and simulation in efficiencies for identifying elec-

Table 1: Summary of the selection criteria used in the SR and CRs. Symbols $\{b\}$ and $\{\ell\}$ refer to cases where the b quark or lepton are not identified. The symbols N_e , N_μ , and N_γ refer to the number of selected electrons, muons, and photons, respectively. The number of b-tagged isolated jets is denoted with $N_{b\text{-tag}}^{\text{iso}}$.

Region	Primary backgrounds	N_e	N_μ	N_γ	$N_{b\text{-tag}}^{\text{iso}}$	CA15 jet b-tag
Signal	$W \rightarrow \{\ell\}\nu,$	0	0	0	0	1
	$Z \rightarrow \nu\nu,$					
	$t\bar{t} \rightarrow \{b\}qq' + b\{\ell\}\nu$					
Targeted contributions						
Single-e (b-tagged)	$t\bar{t} \rightarrow bqq' + b e\nu$	1	0	0	1	1
Single- μ (b-tagged)	$t\bar{t} \rightarrow bqq' + b\mu\nu$	0	1	0	1	1
Single-e (b-vetoed)	$W \rightarrow e\nu$	1	0	0	0	0
Single- μ (b-vetoed)	$W \rightarrow \mu\nu$	0	1	0	0	0
Dielectron	$Z \rightarrow ee$	2	0	0	0	—
Dimuon	$Z \rightarrow \mu\mu$	0	2	0	0	—
Photon	γ	0	0	1	0	—

trons, muons, and photons, correction factors are applied to simulated events in CRs where they are selected.

5.2 Transfer factors

The dominant SM process in each CR is used to estimate at least one background in the SR. Each constraint is encoded through a transfer factor T , which is the ratio of the predicted yield of the targeted process in the SR and its predicted yield in the CR. This factor is defined as a function of p_T^{recoil} and is estimated using simulation. If the CR X is used to estimate the process Y in the SR, then the number of events predicted in bin i of the CR is $N_i^X = \mu_i^Y / T_i^X$, where μ_i^Y is the free parameter of the likelihood representing the number of events from process Y observed in bin i of the SR.

The $t\bar{t}$ and W +jets backgrounds in the SR are estimated using data in the corresponding subsample of the single lepton CRs. Transfer factors ($T^{b\ell}$ and T^ℓ) are obtained from simulations that take into account the effect of lepton acceptances and efficiencies, the b tagging efficiency, and, for the single-electron control sample, the additional p_T^{miss} requirement. These transfer factors explicitly include hadronically decaying τ leptons that fail the identification criteria, which account for roughly 20%–80% of the total W +jets background in the high-recoil region. Because of a large $t\bar{t}$ contamination in the tight W +jets CR, an additional transfer factor is imposed between the $t\bar{t}$ predictions in the b-tagged and b-vetoed single lepton CRs. This provides an estimate of the $t\bar{t}$ contribution in both the SR and the W +jets CRs from the b-tagged CR.

The $Z(\nu\nu)$ +jets background prediction in the SR is determined from the dimuon and dielectron CRs through transfer factors ($T^{\ell\ell}$). They are obtained from simulation and account for the difference in the branching fractions of $Z \rightarrow \nu\nu$ and $Z \rightarrow \ell\ell$ decays and the impacts of lepton acceptance and selection efficiencies. As the branching fraction of the Z boson to electrons and muons is approximately a factor of three smaller than to neutrinos, the resulting constraint on the $Z(\nu\nu)$ +jets background from the dilepton CRs is limited by the statistical uncertainty in the dilepton control samples at large values of p_T^{recoil} .

The γ +jets CR is also used to constrain the $Z(\nu\nu)$ +jets background prediction via a transfer factor T^γ , which accounts for the difference in cross section and the acceptance and efficiency

of identifying photon events. This production mode is similar to that of $Z(\nu\nu)$ +jets, providing thereby a constraint from data on the shape of the predicted $Z p_T$ spectrum. Since the production cross section for γ +jets events is roughly twice that for $Z(\nu\nu)$ +jets events, the addition of this CR to constrain the $Z(\nu\nu)$ +jets background prediction reduces the effect of the limited statistical power of the dilepton events. However, additional theoretical systematic uncertainties are introduced in the extrapolation from this CR to the SR.

A further constraint on the $Z(\nu\nu)$ +jets background is given by W +jets events in the single lepton b-vetoed CRs via $T^{W/Z}$ transfer factors. Additional theoretical uncertainties are included for covering the extrapolation from $W(\ell\nu)$ +jets to $Z(\nu\nu)$ +jets events.

5.3 Systematic uncertainties

The p_T^{recoil} spectra of the processes considered are determined through a binned maximum-likelihood fit, performed simultaneously across all fourteen CRs and two SRs. Systematic uncertainties are treated as nuisance parameters θ that are constrained in the fit.

Uncertainties associated with the transfer factors T^X as a function of p_T^{recoil} are each modeled with a Gaussian prior distribution. They include theoretical uncertainties in the ratio of γ and Z differential cross sections and in the ratio of W and Z differential cross sections, coming from the choice of the renormalization and factorization scales. We also account for variations of T^X due to the PDF uncertainties, following the NNPDF3.0 prescription [26]. We consider uncertainties on T^X associated with the electroweak corrections to γ , Z , and W processes, due to higher-order electroweak effects [21, 23, 43–48]. Each of the uncertainties from renormalization and factorization scales, PDF, and electroweak effects is correlated among bins of p_T^{miss} , but is not correlated among different processes. Finally, uncertainties in the efficiencies of b tagging AK4 jets and subjects are propagated as uncertainties on T^X .

The uncertainties detailed in the following only affect the normalizations of the respective processes and are given a log-normal prior distribution.

An uncertainty of 21% in the heavy-flavor fraction in W +jets events is computed using CMS measurements of inclusive W +jets [49] and W +heavy-flavor [49, 50] production. This is propagated to each of the SRs and the CRs by scaling up and down the heavy-flavor fractions in the prediction by one standard deviation. These W +heavy-flavor uncertainties are correlated among all regions in the fit. A similar method is used for the Z +heavy-flavor fraction uncertainty (22%) using measurements of Z +jets production at CMS [51, 52]. This uncertainty is also correlated among all regions, but is uncorrelated with the W +heavy-flavor uncertainty. The magnitudes of these W/Z +heavy-flavor uncertainties are different for each region (depending on b tagging requirements) and range from 3 to 4% of the nominal W/Z +jets prediction.

Additional uncertainties are included to account for the differences between data and simulation in the CA15 jet m_{SD} and BDT distributions. To derive the uncertainty for top quark jets, the efficiency of the mass window and BDT selection is measured in data using the mass spectrum of CA15 jets observed in a CR that is enriched in $t\bar{t}$ events, where one top quark decays to a muon and jets. Then, variations due to the parton shower algorithm, higher-order corrections, and experimental effects are propagated to the efficiency measurement. This is done for the loose and tight categories independently. The final uncertainty for tagging CA15 jets from a top quark decay is found to be 6% in both categories. Similarly, the uncertainty in mistagging a q/g jet is measured by computing the efficiency in a $Z(\mu\mu)$ +jets selection. The mistag uncertainty is 7%. The CRs used to compute these efficiencies and uncertainties are those shown in Fig. 3. The uncertainties corresponding to the m_{SD} and BDT distributions are only applied to

the signal and minor-background predictions. The same selection is applied in the SR and CRs for the data-driven backgrounds (Z+jets, W+jets, $t\bar{t}$), and so these uncertainties cancel in the transfer factors T^X .

Uncertainties in selection efficiencies amount to 1% per selected muon, electron, or photon, and the uncertainty in the τ lepton veto is 3%. These uncertainties are correlated across all p_T^{recoil} bins. A systematic uncertainty of 20% is ascribed to the single top quark background prediction [53], which is correlated among the SR and the leptonic CRs. An uncertainty of 20% is assigned to the diboson production cross section [54, 55], and is correlated across all channels.

The QCD multijet background is estimated from MC simulation in all regions except for the γ +jets CR, where the prediction is obtained from a jet-to-photon misidentification probability measured in an independent control sample of events in data. An uncertainty of 100% is used for the overall QCD multijet yield. This uncertainty is estimated using a sample enriched in QCD multijet events, obtained by requiring the minimum azimuthal angle between \vec{p}_T^{miss} and the AK4 jet directions to be less than 0.1 rad.

For processes estimated from MC simulation, p_T^{miss} uncertainties are obtained directly from simulation and propagated to p_T^{recoil} following the standard CMS method [56], which includes the application of uncertainties in jet energy corrections applied to AK4 jets and p_T^{miss} [32]. The uncertainty in p_T^{miss} is used again as an uncertainty in the normalization in the final fit.

A systematic uncertainty of 2.5% [28] in the integrated luminosity is included for all processes that are estimated using MC simulation.

The impact of statistical uncertainties on the predictions for simulation-driven backgrounds is negligible. For the transfer factors T^X , which are obtained from simulation and used to derive a data-driven estimate of the main backgrounds, we introduce additional nuisance parameters corresponding to bin-by-bin statistical uncertainties.

We further consider uncertainties in the signal cross sections, estimated by observing the effect of varying the renormalization and factorization scales by factors of 0.5 and 2.0, and of the PDF uncertainties. To that end, an uncertainty of 10% is assigned to the nonresonant signal cross sections. The corresponding uncertainties in the resonant signal cross sections vary from 10% to 32% as a function of the mass of the scalar mediator. Unlike other uncertainties, these are not propagated as nuisance parameters, but rather treated as uncertainties in the inclusive signal cross section.

6 Results

Figures 4–7 show the results of the simultaneous fit in all fourteen control regions and two signal regions. The distributions observed in all CRs agree with predictions. Figure 8 shows the distribution in p_T^{miss} in the signal region under the background-only hypothesis. Data are found to be in agreement with the SM prediction. The fit does not require any nuisance parameter to vary more than 1.2 standard deviations from its initial value.

The results of the search are first interpreted in terms of the simplified model for monotop production via an FCNC. Expected and observed limits at 95% confidence level (CL) are set using the asymptotic approximation [57] of the CL_s criterion [58, 59] with a profile likelihood ratio as the test statistic, in which systematic uncertainties are modeled as nuisance parameters. Figure 9 shows the exclusion as a function of the mediator mass m_V and DM particle mass m_χ , assuming $g_q^V = 0.25$, $g_\chi^V = 1$, and $g_q^A = g_\chi^A = 0$. At $m_\chi < 100$ GeV, we observe that the result

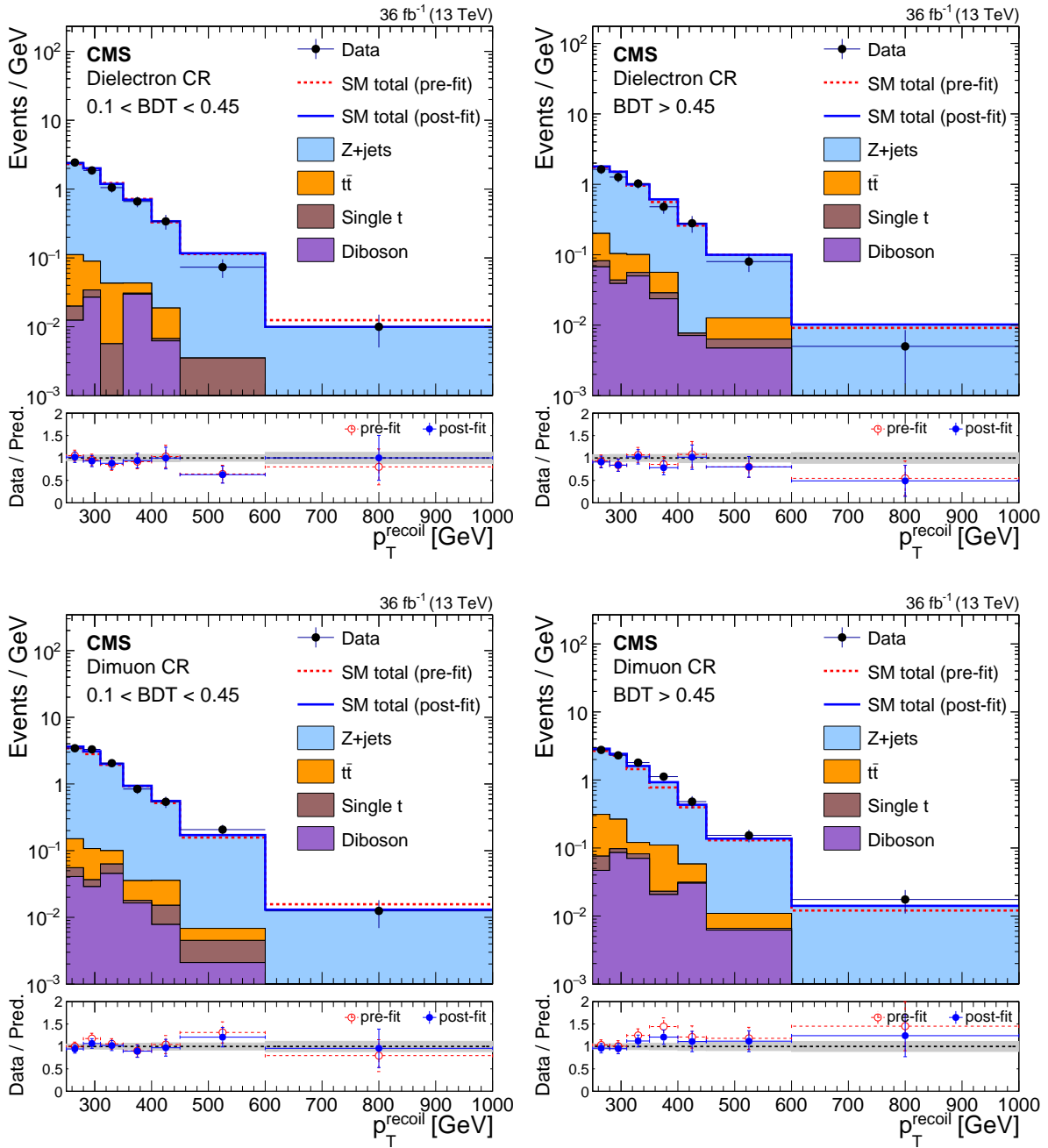


Figure 4: Comparison between data and SM predictions in the dilepton control regions before and after performing the simultaneous fit to the different control regions and signal region. Each bin shows the event yields divided by the width of the bin. The upper row of figures corresponds to the dielectron control region, and the lower row to the dimuon control region. The left (right) column of figures corresponds to the loose (tight) category of the control regions. The blue solid line represents the sum of the SM contributions normalized to their fitted yields. The red dashed line represents the sum of the SM contributions normalized to the prediction. The stacked histograms show the individual fitted SM contributions. The lower panel of each figure shows the ratio of data to fitted prediction. The gray band on the ratio indicates the one standard deviation uncertainty on the prediction after propagating all the systematic uncertainties and their correlations in the fit.

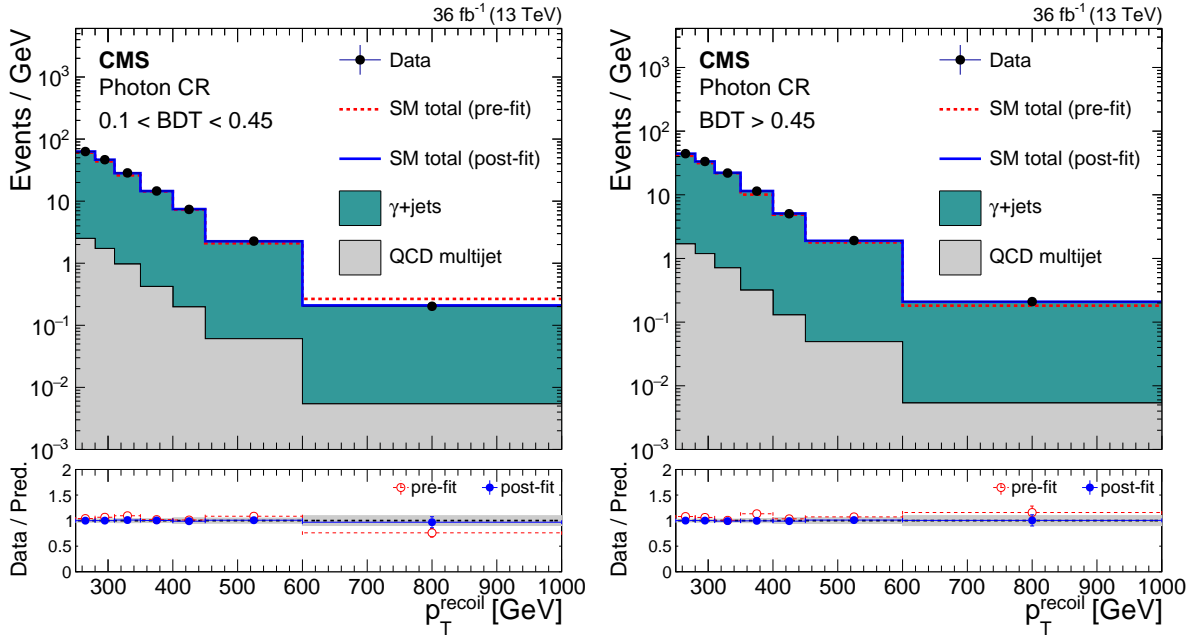


Figure 5: Comparison between data and SM predictions in the photon control regions before and after performing the simultaneous fit to the different control regions and signal region. Each bin shows the event yields divided by the width of the bin. The left (right) figure corresponds to the loose (tight) category of the control region. The blue solid line represents the sum of the SM contributions normalized to their fitted yields. The red dashed line represents the sum of the SM contributions normalized to the prediction. The stacked histograms show the individual fitted SM contributions. The lower panel of each figure shows the ratio of data to fitted prediction. The gray band on the ratio indicates the one standard deviation uncertainty on the prediction after propagating all the systematic uncertainties and their correlations in the fit.

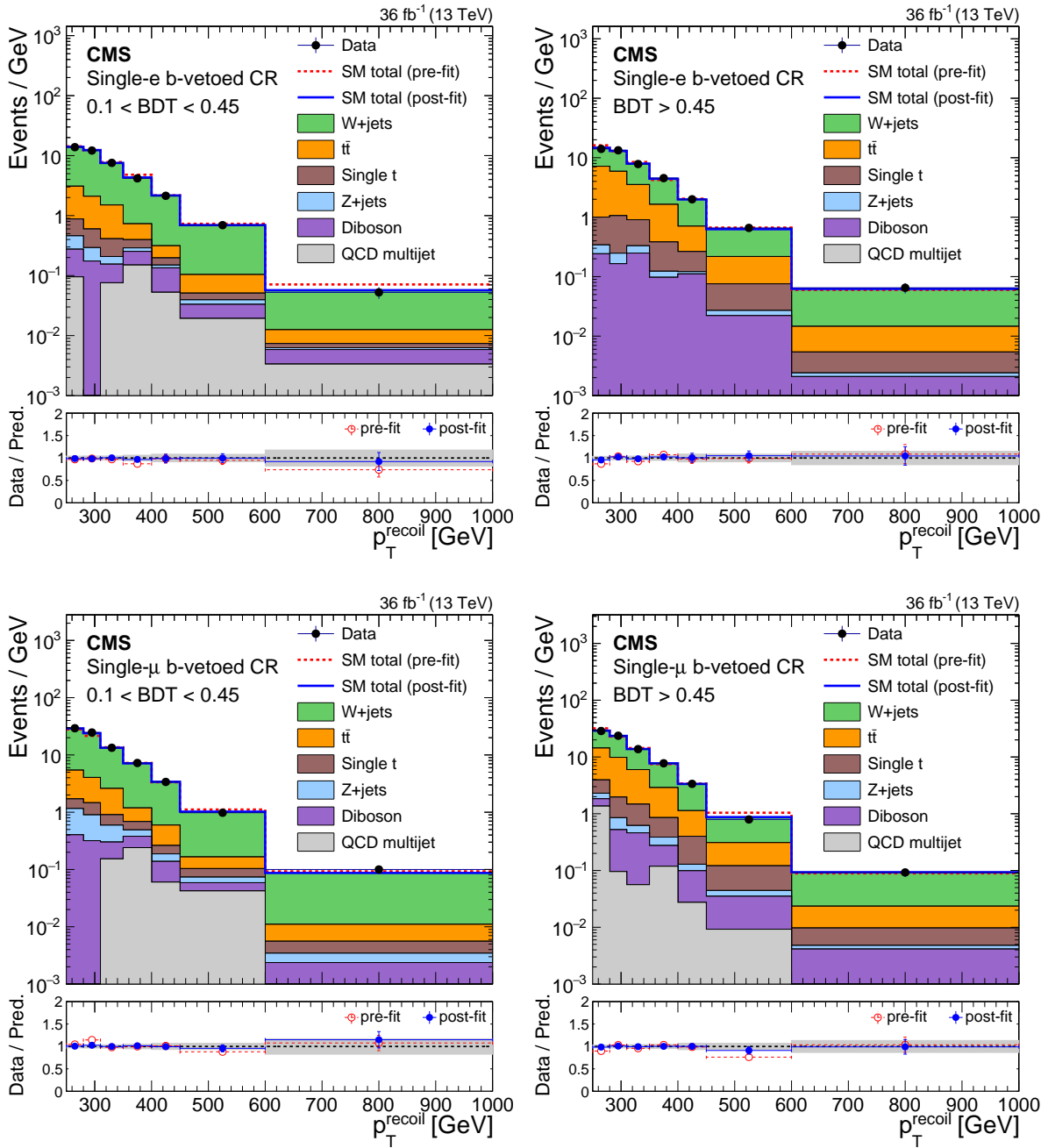


Figure 6: Comparison between data and SM predictions in the b-vetoed single lepton control regions before and after performing the simultaneous fit to the different control regions and signal region. Each bin shows the event yields divided by the width of the bin. The upper row of figures corresponds to the single electron b-vetoed control region, and lower row to the single muon b-vetoed control region. The left (right) column of figures corresponds to the loose (tight) category of the control regions. The blue solid line represents the sum of the SM contributions normalized to their fitted yields. The red dashed line represents the sum of the SM contributions normalized to the prediction. The stacked histograms show the individual fitted SM contributions. The lower panel of each figure shows the ratio of data to fitted prediction. The gray band on the ratio indicates the one standard deviation uncertainty on the prediction after propagating all the systematic uncertainties and their correlations in the fit.

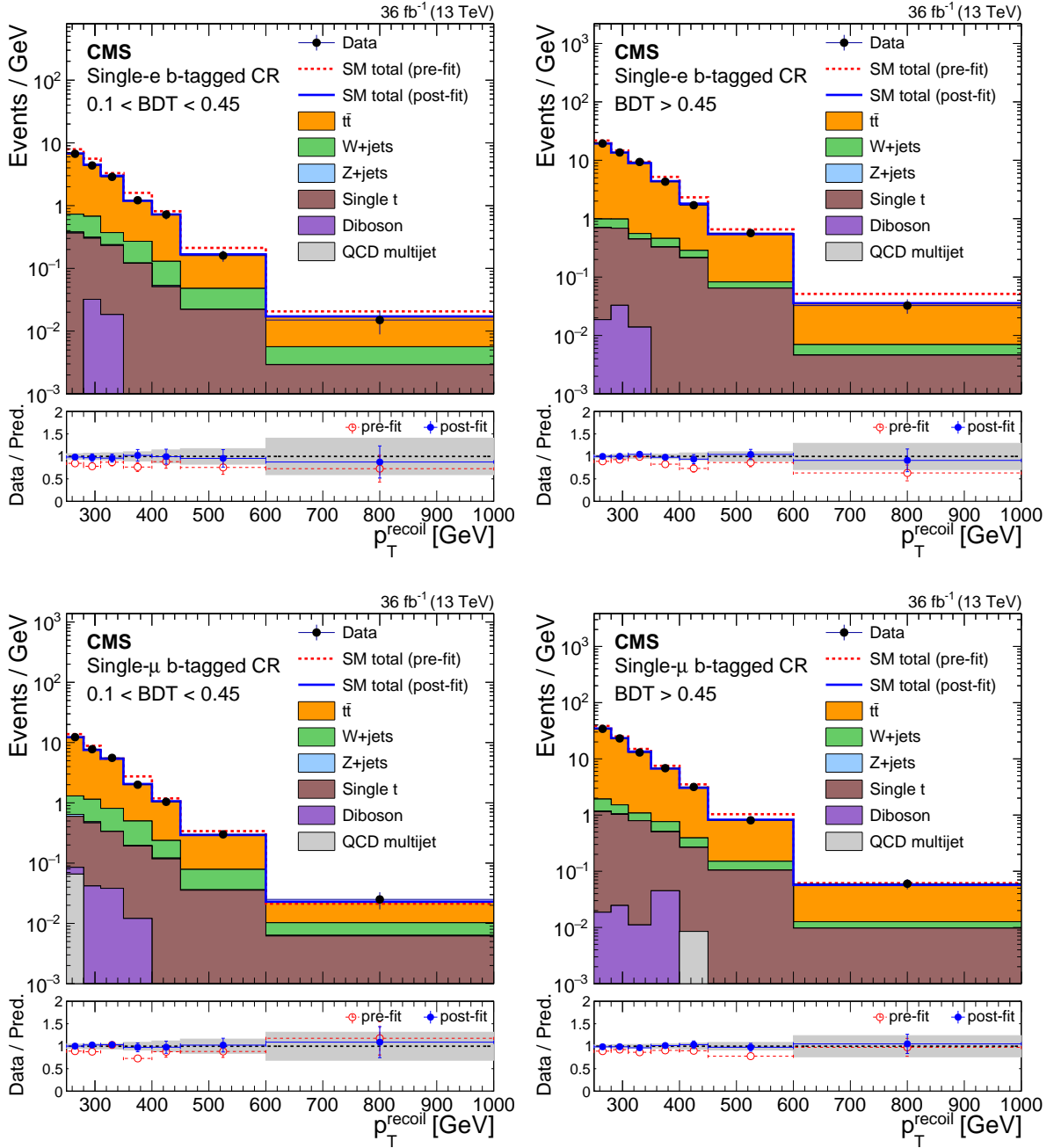


Figure 7: Comparison between data and SM predictions in the b-tagged single lepton control regions before and after performing the simultaneous fit to the different control regions and signal region. Each bin shows the event yields divided by the width of the bin. The upper row of figures corresponds to the single electron b-tagged control region, and lower row to the single muon b-tagged control region. The left (right) column of figures corresponds to the loose (tight) category of the control regions. The blue solid line represents the sum of the SM contributions normalized to their fitted yields. The red dashed line represents the sum of the SM contributions normalized to the prediction. The stacked histograms show the individual fitted SM contributions. The lower panel of each figure shows the ratio of data to fitted prediction. The gray band on the ratio indicates the one standard deviation uncertainty on the prediction after propagating all the systematic uncertainties and their correlations in the fit.

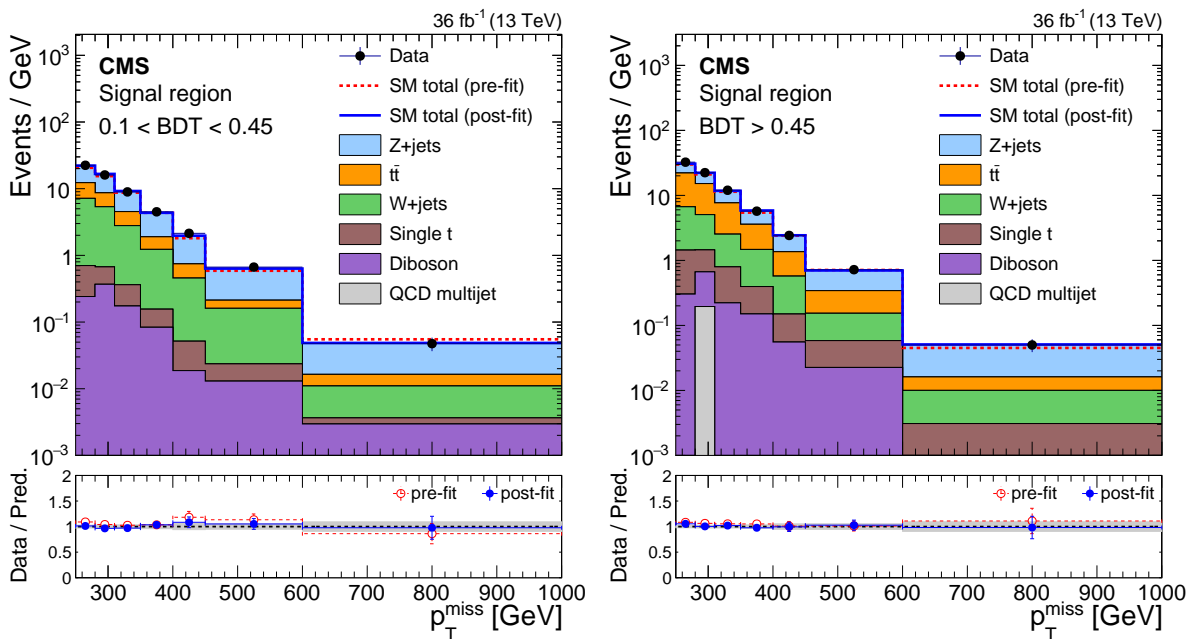


Figure 8: Distribution of p_T^{miss} from SM backgrounds and data in the signal region after simultaneously fitting the signal region and all control regions. Each bin shows the event yields divided by the width of the bin. The left (right) figure corresponds to the loose (tight) category of the signal region. The stacked histograms show the individual fitted SM background contributions. The blue solid line represents the sum of the SM background contributions normalized to their fitted yields. The red dashed line represents the sum of the SM background contributions normalized to the prediction. The lower panel of each figure shows the ratio of data to fitted prediction. The gray band on the ratio indicates the one standard deviation uncertainty on the prediction after propagating all the systematic uncertainties and their correlations in the fit.

is roughly independent of m_χ , and the range $0.2 < m_V < 1.75$ TeV is excluded. This can be compared to an expected exclusion of $0.2 < m_V < 1.78$ TeV. At very high m_χ (i.e., $2m_\chi \gg m_V$), the parameter space is not excluded because the available phase space for the decay to DM decreases in this region. Figure 10 shows an analogous result, obtained with the assumptions $g_q^A = 0.25$, $g_\chi^A = 1$, and $g_q^V = g_\chi^V = 0$. At $m_\chi \sim 1$ GeV, the result in the axial case is very similar to the vector case. An exclusion of $0.2 < m_V < 1.75$ TeV is obtained for the FCNCs, compared to an expected exclusion of $0.2 < m_V < 1.78$ TeV. However, as m_χ approaches the off-shell region, the shape of the exclusion is modified owing to the coupling structure.

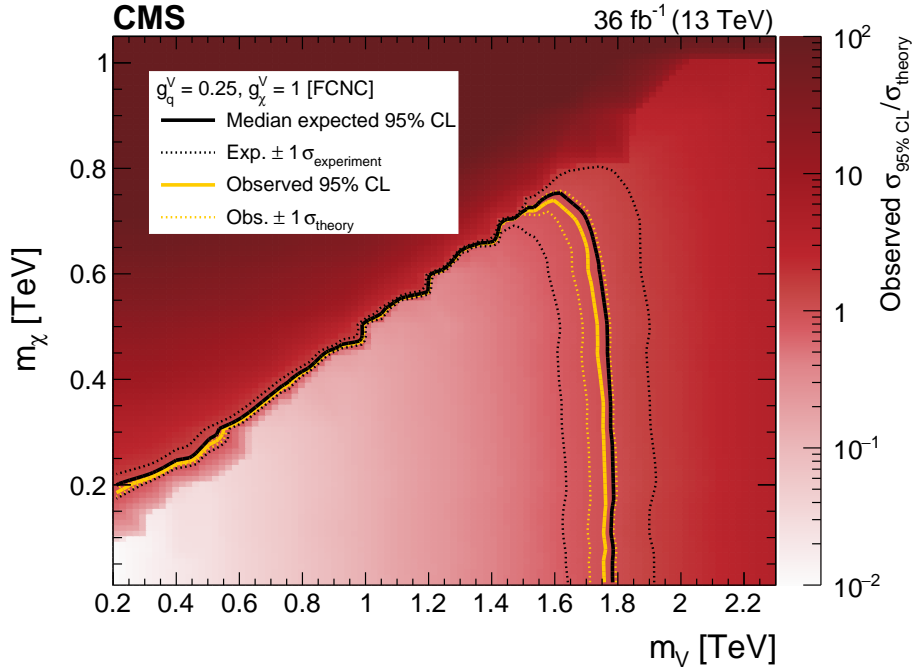


Figure 9: Results for the FCNC interpretation presented in the two-dimensional plane spanned by the mediator and DM masses. The mediator is assumed to have purely vector couplings to quarks and DM particles. The observed exclusion range (gold solid line) is shown. The gold dashed lines show the cases in which the predicted cross section is shifted by the assigned theoretical uncertainty. The expected exclusion range is indicated by a black solid line, demonstrating the search sensitivity of the analysis. The experimental uncertainties are shown in black dashed lines.

In addition to considering the dependence on the DM and mediator masses, limits are calculated as a function of the couplings between DM and the mediator, and between quarks and the mediator. We fix $m_\chi = 1$ GeV and show the 95% CL exclusion in the planes spanned by the couplings and m_V , assuming vector- (Fig. 11) and axial-only couplings (Fig. 12). Very little difference is observed between the two coupling schemes. At low mediator and DM masses, coupling combinations as small as $g_\chi^{V,A} = 0.05$, $g_q^{V,A} = 0.25$ and $g_\chi^{V,A} = 1$, $g_q^{V,A} = 0.05$ are excluded. Fig. A.7 in Appendix A shows the maximum excluded m_V as a function of g_χ^V and g_q^V .

Figure 13 shows the results in the resonant model interpretation. The DM mass is fixed at $m_\psi = 100$ GeV, and the couplings are assumed to be $a_q = b_q = 0.1$ and $a_\psi = b_\psi = 0.2$. Scalars with mass $1.5 < m_\phi < 3.4$ TeV are excluded at 95% CL.

A summary of the importance of the systematic uncertainties is presented in Table A.1. To

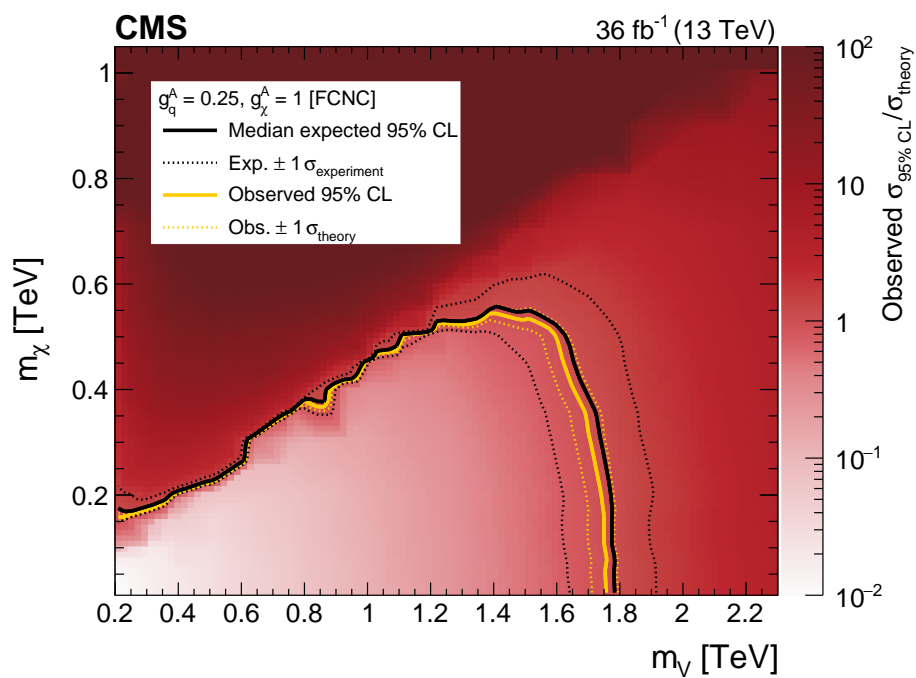


Figure 10: Results for the FCNC interpretation presented in the two-dimensional plane spanned by the mediator and DM masses. The mediator is assumed to have purely axial couplings to quarks and DM particles. The observed exclusion range (gold solid line) is shown. The gold dashed lines show the cases in which the predicted cross section is shifted by the assigned theoretical uncertainty. The expected exclusion range is indicated by a black solid line, demonstrating the search sensitivity of the analysis. The experimental uncertainties are shown in black dashed lines.

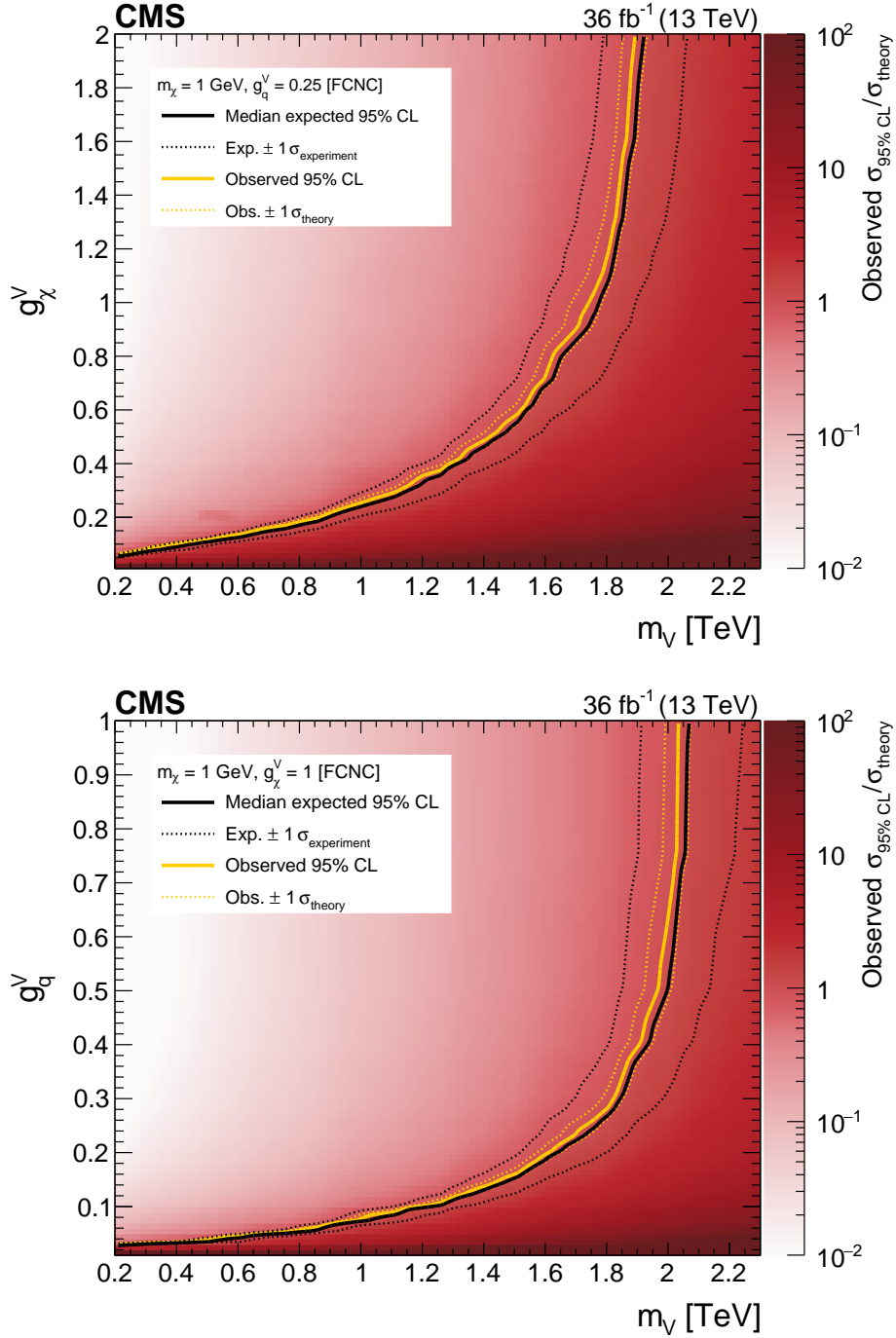


Figure 11: Results for the FCNC interpretation presented in the two-dimensional plane spanned by the mediator mass and the coupling between the mediator and DM (upper) or quarks (lower). The mediator is assumed to have purely vector couplings. The observed exclusion range (gold solid line) is shown. The gold dashed lines show the cases in which the predicted cross section is shifted by the assigned theoretical uncertainty. The expected exclusion range is indicated by a black solid line, demonstrating the search sensitivity of the analysis. The experimental uncertainties are shown in black dashed lines.

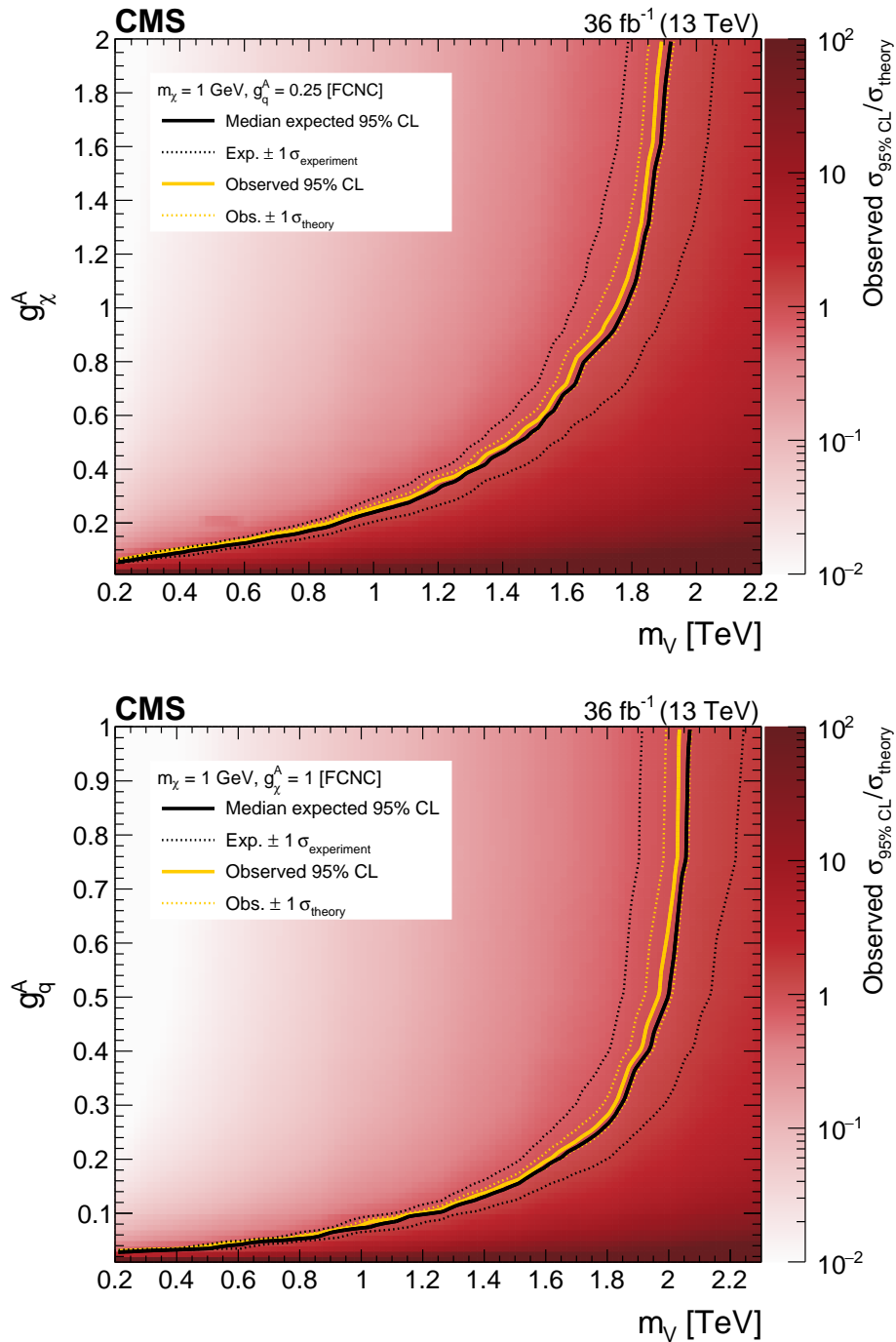


Figure 12: Results for the FCNC interpretation presented in the two-dimensional plane spanned by the mediator mass and the coupling between the mediator and DM (upper) or quarks (lower). The mediator is assumed to have purely axial couplings. The observed exclusion range (gold solid line) is shown. The gold dashed lines show the cases in which the predicted cross section is shifted by the assigned theoretical uncertainty. The expected exclusion range is indicated by a black solid line, demonstrating the search sensitivity of the analysis. The experimental uncertainties are shown in black dashed lines.

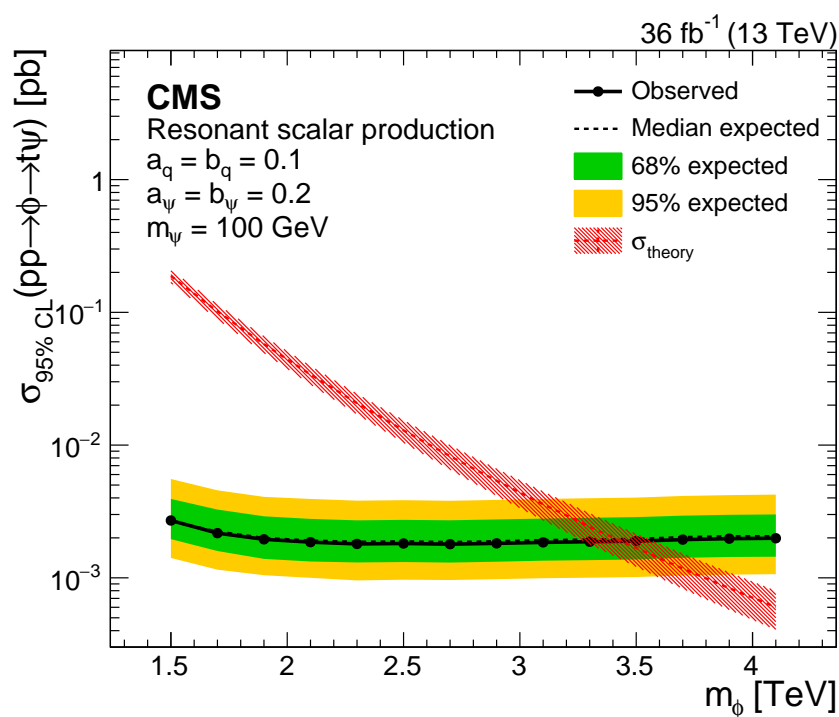


Figure 13: Upper limits at 95% CL on the mass of the scalar particle ϕ in the resonant model, assuming fixed $a_q = b_q = 0.1$ and $a_\psi = b_\psi = 0.2$. The green and yellow bands represent one and two standard deviations of experimental uncertainties, respectively. The red hatched band represents the signal cross section uncertainty as a function of m_ϕ .

allow for reinterpretation of the data in the context of signal models not considered in this paper, we provide the results of fitting data in the CRs and propagating the prediction to the SRs in Appendix A (Fig. A.3-A.6 and Tables A.2-A.3).

7 Summary

A search is reported for dark matter events with large transverse momentum imbalance and a hadronically decaying top quark. New t tagging techniques are presented and utilized to identify jets from the Lorentz-boosted top quark. The data are found to be in agreement with the standard model prediction for the expected background. Results are interpreted in terms of limits on the production cross section of dark matter (DM) particles via a flavor-changing neutral current interaction or via the decay of a colored scalar resonance.

Other experimental searches [60] probe the production of DM via neutral currents, under the assumption that flavor is conserved. This analysis augments these searches by considering DM production in scenarios that violate flavor conservation. Assuming $m_\chi = 1$ GeV, $g_u^V = 0.25$, and $g_\chi^V = 1$, spin-1 mediators with masses $0.2 < m_V < 1.75$ TeV in the FCNC model are excluded at the 95% confidence level. Scalar resonances decaying to DM and a top quark are excluded in the range $1.5 < m_\phi < 3.4$ TeV, assuming $m_\psi = 100$ GeV.

Acknowledgments

We congratulate our colleagues in the CERN accelerator departments for the excellent performance of the LHC and thank the technical and administrative staffs at CERN and at other CMS institutes for their contributions to the success of the CMS effort. In addition, we gratefully acknowledge the computing centers and personnel of the Worldwide LHC Computing Grid for delivering so effectively the computing infrastructure essential to our analyses. Finally, we acknowledge the enduring support for the construction and operation of the LHC and the CMS detector provided by the following funding agencies: BMWFW and FWF (Austria); FNRS and FWO (Belgium); CNPq, CAPES, FAPERJ, and FAPESP (Brazil); MES (Bulgaria); CERN; CAS, MoST, and NSFC (China); COLCIENCIAS (Colombia); MSES and CSF (Croatia); RPF (Cyprus); SENESCYT (Ecuador); MoER, ERC IUT, and ERDF (Estonia); Academy of Finland, MEC, and HIP (Finland); CEA and CNRS/IN2P3 (France); BMBF, DFG, and HGF (Germany); GSRT (Greece); OTKA and NIH (Hungary); DAE and DST (India); IPM (Iran); SFI (Ireland); INFN (Italy); MSIP and NRF (Republic of Korea); LAS (Lithuania); MOE and UM (Malaysia); BUAP, CINVESTAV, CONACYT, LNS, SEP, and UASLP-FAI (Mexico); MBIE (New Zealand); PAEC (Pakistan); MSHE and NSC (Poland); FCT (Portugal); JINR (Dubna); MON, RosAtom, RAS, RFBR and RAEP (Russia); MESTD (Serbia); SEIDI, CPAN, PCTI and FEDER (Spain); Swiss Funding Agencies (Switzerland); MST (Taipei); ThEPCenter, IPST, STAR, and NSTDA (Thailand); TUBITAK and TAEK (Turkey); NASU and SFFR (Ukraine); STFC (United Kingdom); DOE and NSF (USA).

Individuals have received support from the Marie-Curie program and the European Research Council and Horizon 2020 Grant, contract No. 675440 (European Union); the Leventis Foundation; the A. P. Sloan Foundation; the Alexander von Humboldt Foundation; the Belgian Federal Science Policy Office; the Fonds pour la Formation à la Recherche dans l'Industrie et dans l'Agriculture (FRIA-Belgium); the Agentschap voor Innovatie door Wetenschap en Technologie (IWT-Belgium); the Ministry of Education, Youth and Sports (MEYS) of the Czech Republic; the Council of Science and Industrial Research, India; the HOMING PLUS program of the Foundation for Polish Science, cofinanced from European Union, Regional Development Fund, the

Mobility Plus program of the Ministry of Science and Higher Education, the National Science Center (Poland), contracts Harmonia 2014/14/M/ST2/00428, Opus 2014/13/B/ST2/02543, 2014/15/B/ST2/03998, and 2015/19/B/ST2/02861, Sonata-bis 2012/07/E/ST2/01406; the National Priorities Research Program by Qatar National Research Fund; the Programa Severo Ochoa del Principado de Asturias; the Thalys and Aristeia programs cofinanced by EU-ESF and the Greek NSRF; the Rachadapisek Sompot Fund for Postdoctoral Fellowship, Chulalongkorn University and the Chulalongkorn Academic into Its 2nd Century Project Advancement Project (Thailand); the Welch Foundation, contract C-1845; and the Weston Havens Foundation (USA).

We thank Benjamin Fuks for his help in devising the signal models used in the interpretation of the results.

References

- [1] G. Bertone, D. Hooper, and J. Silk, “Particle dark matter: evidence, candidates and constraints”, *Physics Reports* **405** (2005) 279, doi:10.1016/j.physrep.2004.08.031.
- [2] J. L. Feng, “Dark matter candidates from particle physics and methods of detection”, *Ann. Rev. Astron. Astrophys.* **48** (2010) 495, doi:10.1146/annurev-astro-082708-101659, arXiv:1003.0904.
- [3] T. A. Porter, R. P. Johnson, and P. W. Graham, “Dark matter searches with astroparticle data”, *Ann. Rev. Astron. Astrophys.* **49** (2011) 15, doi:10.1146/annurev-astro-081710-102528, arXiv:1104.2836.
- [4] LUX Collaboration, “The Large Underground Xenon (LUX) experiment”, *Nucl. Instrum. Meth. A* **704** (2013) 111, doi:10.1016/j.nima.2012.11.135, arXiv:1211.3788.
- [5] AMS Collaboration, “Electron and positron fluxes in primary cosmic rays measured with the alpha magnetic spectrometer on the international space station”, *Phys. Rev. Lett.* **113** (2014) 121102, doi:10.1103/PhysRevLett.113.121102.
- [6] J. Andrea, B. Fuks, and F. Maltoni, “Monotops at the LHC”, *Phys. Rev. D* **84** (2011) 074025, doi:10.1103/PhysRevD.84.074025, arXiv:1106.6199.
- [7] CDF Collaboration, “Search for a dark matter candidate produced in association with a single top quark in $p\bar{p}$ collisions at $\sqrt{s} = 1.96$ TeV”, *Phys. Rev. Lett.* **108** (2012) 201802, doi:10.1103/PhysRevLett.108.201802, arXiv:1202.5653.
- [8] CMS Collaboration, “Search for monotop signatures in proton-proton collisions at $\sqrt{s} = 8$ TeV”, *Phys. Rev. Lett.* **114** (2015) 101801, doi:10.1103/PhysRevLett.114.101801, arXiv:1410.1149.
- [9] ATLAS Collaboration, “Search for invisible particles produced in association with single-top-quarks in proton-proton collisions at $\sqrt{s} = 8$ TeV with the ATLAS detector”, *Eur. Phys. J. C* **75** (2015) 79, doi:10.1140/epjc/s10052-014-3233-4, arXiv:1410.5404.
- [10] J.-L. Agram et al., “Monotop phenomenology at the Large Hadron Collider”, *Phys. Rev. D* **89** (2014) 014028, doi:10.1103/PhysRevD.89.014028, arXiv:1311.6478.
- [11] I. Boucheneb, G. Cacciapaglia, A. Deandrea, and B. Fuks, “Revisiting monotop production at the LHC”, *JHEP* **01** (2015) 017, doi:10.1007/JHEP01(2015)017, arXiv:1407.7529.
- [12] CMS Collaboration, “The CMS experiment at the CERN LHC”, *JINST* **3** (2008) S08004, doi:10.1088/1748-0221/3/08/S08004.
- [13] CMS Collaboration, “Particle-flow reconstruction and global event description with the CMS detector”, *JINST* **12** (2017) P10003, doi:10.1088/1748-0221/12/10/P10003, arXiv:1706.04965.
- [14] J. Alwall et al., “The automated computation of tree-level and next-to-leading order differential cross sections, and their matching to parton shower simulations”, *JHEP* **07** (2014) 079, doi:10.1007/JHEP07(2014)079, arXiv:1405.0301.

-
- [15] P. Nason, “A new method for combining NLO QCD with shower Monte Carlo algorithms”, *JHEP* **11** (2004) 040, doi:10.1088/1126-6708/2004/11/040, arXiv:hep-ph/0409146.
- [16] S. Frixione, P. Nason, and C. Oleari, “Matching NLO QCD computations with parton shower simulations: the POWHEG method”, *JHEP* **11** (2007) 070, doi:10.1088/1126-6708/2007/11/070, arXiv:0709.2092.
- [17] S. Alioli, P. Nason, C. Oleari, and E. Re, “A general framework for implementing NLO calculations in shower Monte Carlo programs: the POWHEG BOX”, *JHEP* **06** (2010) 043, doi:10.1007/JHEP06(2010)043, arXiv:1002.2581.
- [18] T. Sjöstrand et al., “An introduction to PYTHIA 8.2”, *Comput. Phys. Commun.* **191** (2015) 159, doi:10.1016/j.cpc.2015.01.024, arXiv:1410.3012.
- [19] J. Alwall et al., “Comparative study of various algorithms for the merging of parton showers and matrix elements in hadronic collisions”, *Eur. Phys. J. C* **53** (2008) 473, doi:10.1140/epjc/s10052-007-0490-5, arXiv:0706.2569.
- [20] R. Frederix and S. Frixione, “Merging meets matching in MC@NLO”, *JHEP* **12** (2012) 061, doi:10.1007/JHEP12(2012)061, arXiv:1209.6215.
- [21] J. H. Kuhn, A. Kulesza, S. Pozzorini, and M. Schulze, “Electroweak corrections to hadronic photon production at large transverse momenta”, *JHEP* **03** (2006) 059, doi:10.1088/1126-6708/2006/03/059, arXiv:hep-ph/0508253.
- [22] S. Kallweit et al., “NLO QCD+EW automation and precise predictions for V+multijet production”, in *50th Rencontres de Moriond on QCD and High Energy Interactions La Thuile, Italy, March 21-28, 2015*. 2015. arXiv:1505.05704.
- [23] S. Kallweit et al., “NLO QCD+EW predictions for V + jets including off-shell vector-boson decays and multijet merging”, *JHEP* **04** (2016) 021, doi:10.1007/JHEP04(2016)021, arXiv:1511.08692.
- [24] CMS Collaboration, “Event generator tunes obtained from underlying event and multiparton scattering measurements”, *Eur. Phys. J. C* **76** (2016) 155, doi:10.1140/epjc/s10052-016-3988-x, arXiv:1512.00815.
- [25] P. Skands, S. Carrazza, and J. Rojo, “Tuning PYTHIA 8.1: the Monash 2013 tune”, *Eur. Phys. J. C* **74** (2014) 3024, doi:10.1140/epjc/s10052-014-3024-y, arXiv:1404.5630.
- [26] NNPDF Collaboration, “Parton distributions for the LHC Run II”, *JHEP* **04** (2015) 040, doi:10.1007/JHEP04(2015)040, arXiv:1410.8849.
- [27] GEANT4 Collaboration, “GEANT4—a simulation toolkit”, *Nucl. Instrum. Meth. A* **506** (2003) 250, doi:10.1016/S0168-9002(03)01368-8.
- [28] CMS Collaboration, “CMS luminosity measurements for the 2016 data taking period”, CMS Physics Analysis Summary CMS-PAS-LUM-17-001, 2017.
- [29] M. Cacciari, G. P. Salam, and G. Soyez, “The anti- k_t jet clustering algorithm”, *JHEP* **04** (2008) 063, doi:10.1088/1126-6708/2008/04/063, arXiv:0802.1189.

- [30] Y. L. Dokshitzer, G. D. Leder, S. Moretti, and B. R. Webber, “Better jet clustering algorithms”, *JHEP* **08** (1997) 001, doi:10.1088/1126-6708/1997/08/001, arXiv:hep-ph/9707323.
- [31] D. Bertolini, P. Harris, M. Low, and N. Tran, “Pileup per particle identification”, *JHEP* **10** (2014) 59, doi:10.1007/JHEP10(2014)059.
- [32] CMS Collaboration, “Jet energy scale and resolution in the CMS experiment in pp collisions at 8 TeV”, *JINST* **12** (2017) P02014, doi:10.1088/1748-0221/12/02/P02014, arXiv:1607.03663.
- [33] A. J. Larkoski, S. Marzani, G. Soyez, and J. Thaler, “Soft drop”, *JHEP* **05** (2014) 146, doi:10.1007/JHEP05(2014)146, arXiv:1402.2657.
- [34] CMS Collaboration, “Identification of b-quark jets with the CMS experiment”, *JINST* **8** (2012) P04013, doi:10.1088/1748-0221/8/04/P04013.
- [35] CMS Collaboration, “Identification of b quark jets at the CMS Experiment in the LHC Run 2”, CMS Physics Analysis Summary CMS-PAS-BTV-15-001, 2016.
- [36] H. Voss, A. Höcker, J. Stelzer, and F. Tegenfeldt, “TMVA, the toolkit for multivariate data analysis with ROOT”, in *XIth International Workshop on Advanced Computing and Analysis Techniques in Physics Research (ACAT)*, p. 40. 2007. arXiv:physics/0703039.
- [37] J. Thaler and K. Tilburg, “Identifying boosted objects with N -subjettiness”, *JHEP* **03** (2011) 015, doi:10.1007/JHEP03(2011)015, arXiv:1011.2268.
- [38] C. Anders et al., “Benchmarking an even better top tagger algorithm”, *Phys. Rev. D* **89** (2014) 074047, doi:10.1103/PhysRevD.89.074047, arXiv:1312.1504.
- [39] A. J. Larkoski, G. P. Salam, and J. Thaler, “Energy correlation functions for jet substructure”, *JHEP* **06** (2013) 108, doi:10.1007/JHEP06(2013)108, arXiv:1305.0007.
- [40] I. Moutl, L. Necib, and J. Thaler, “New angles on energy correlation functions”, *JHEP* **12** (2016) 153, doi:10.1007/JHEP12(2016)153, arXiv:1609.07483.
- [41] CMS Collaboration, “Performance of electron reconstruction and selection with the CMS detector in proton-proton collisions at $\sqrt{s} = 8$ TeV”, *JINST* **10** (2015) P06005, doi:10.1088/1748-0221/10/06/P06005, arXiv:1502.02701.
- [42] CMS Collaboration, “Performance of photon reconstruction and identification with the CMS detector in proton-proton collisions at $\sqrt{s} = 8$ TeV”, *JINST* **10** (2015) P08010, doi:10.1088/1748-0221/10/08/P08010, arXiv:1502.02702.
- [43] A. Denner, S. Dittmaier, T. Kasprzik, and A. Muck, “Electroweak corrections to $W +$ jet hadroproduction including leptonic W -boson decays”, *JHEP* **08** (2009) 075, doi:10.1088/1126-6708/2009/08/075, arXiv:0906.1656.
- [44] A. Denner, S. Dittmaier, T. Kasprzik, and A. Muck, “Electroweak corrections to dilepton + jet production at hadron colliders”, *JHEP* **06** (2011) 069, doi:10.1007/JHEP06(2011)069, arXiv:1103.0914.
- [45] A. Denner, S. Dittmaier, T. Kasprzik, and A. Mück, “Electroweak corrections to monojet production at the LHC”, *Eur. Phys. J. C* **73** (2013) 2297, doi:10.1140/epjc/s10052-013-2297-x, arXiv:1211.5078.

- [46] J. H. Kuhn, A. Kulesza, S. Pozzorini, and M. Schulze, “Logarithmic electroweak corrections to hadronic Z+1 jet production at large transverse momentum”, *Phys. Lett. B* **609** (2005) 277, doi:10.1016/j.physletb.2005.01.059, arXiv:hep-ph/0408308.
- [47] J. H. Kuhn, A. Kulesza, S. Pozzorini, and M. Schulze, “One-loop weak corrections to hadronic production of Z bosons at large transverse momenta”, *Nucl. Phys. B* **727** (2005) 368, doi:10.1016/j.nuclphysb.2005.08.019, arXiv:hep-ph/0507178.
- [48] J. H. Kuhn, A. Kulesza, S. Pozzorini, and M. Schulze, “Electroweak corrections to hadronic production of W bosons at large transverse momenta”, *Nucl. Phys. B* **797** (2008) 27, doi:10.1016/j.nuclphysb.2007.12.029, arXiv:0708.0476.
- [49] CMS Collaboration, “Differential cross section measurements for the production of a W boson in association with jets in proton-proton collisions at $\sqrt{s} = 7$ TeV”, *Phys. Lett. B* **741** (2015) 12, doi:10.1016/j.physletb.2014.12.003, arXiv:1406.7533.
- [50] CMS Collaboration, “Measurement of the production cross section for a W boson and two b jets in pp collisions at $\sqrt{s}=7$ TeV”, *Phys. Lett. B* **735** (2014) 204, doi:10.1016/j.physletb.2014.06.041, arXiv:1312.6608.
- [51] CMS Collaboration, “Measurements of jet multiplicity and differential production cross sections of Z+ jets events in proton-proton collisions at $\sqrt{s} = 7$ TeV”, *Phys. Rev. D* **91** (2015) 052008, doi:10.1103/PhysRevD.91.052008, arXiv:1408.3104.
- [52] CMS Collaboration, “Measurement of the production cross sections for a Z boson and one or more b jets in pp collisions at $\sqrt{s} = 7$ TeV”, *JHEP* **06** (2014) 120, doi:10.1007/JHEP06(2014)120, arXiv:1402.1521.
- [53] CMS Collaboration, “Observation of the associated production of a single top quark and a W boson in pp collisions at $\sqrt{s} = 8$ TeV”, *Phys. Rev. Lett.* **112** (2014) 231802, doi:10.1103/PhysRevLett.112.231802, arXiv:1401.2942.
- [54] CMS Collaboration, “Measurement of the ZZ production cross section and $Z \rightarrow \ell^+ \ell^- \ell'^+ \ell'^-$ branching fraction in pp collisions at $\sqrt{s} = 13$ TeV”, *Phys. Lett. B* **763** (2016) 280, doi:10.1016/j.physletb.2016.10.054, arXiv:1607.08834.
- [55] CMS Collaboration, “Measurement of the WZ production cross section in pp collisions at $\sqrt{s} = 13$ TeV”, *Phys. Lett. B* **766** (2017) 268, doi:10.1016/j.physletb.2017.01.011, arXiv:1607.06943.
- [56] CMS Collaboration, “Performance of the CMS missing transverse momentum reconstruction in pp data at $\sqrt{s} = 8$ TeV”, *JINST* **10** (2015) P02006, doi:10.1088/1748-0221/10/02/P02006, arXiv:1411.0511.
- [57] G. Cowan, K. Cranmer, E. Gross, and O. Vitells, “Asymptotic formulae for likelihood-based tests of new physics”, *Eur. Phys. J. C* **71** (2011) 1554, doi:10.1140/epjc/s10052-011-1554-0, arXiv:1007.1727. [Erratum: doi:10.1140/epjc/s10052-013-2501-z].
- [58] T. Junk, “Confidence level computation for combining searches with small statistics”, *Nucl. Instrum. Meth. A* **434** (1999) 435, doi:10.1016/S0168-9002(99)00498-2.

-
- [59] A. L. Read, "Presentation of search results: the CL_s technique", in *Durham IPPP Workshop: Advanced Statistical Techniques in Particle Physics*, p. 2693. Durham, UK, March, 2002. [*J. Phys. G* 28 (2002) 2693]. doi:10.1088/0954-3899/28/10/313.
- [60] CMS Collaboration, "Search for dark matter produced with an energetic jet or a hadronically decaying W or Z boson at $\sqrt{s} = 13$ TeV", *JHEP* 07 (2017) 014, doi:10.1007/JHEP07(2017)014, arXiv:1703.01651.

A Supplementary material

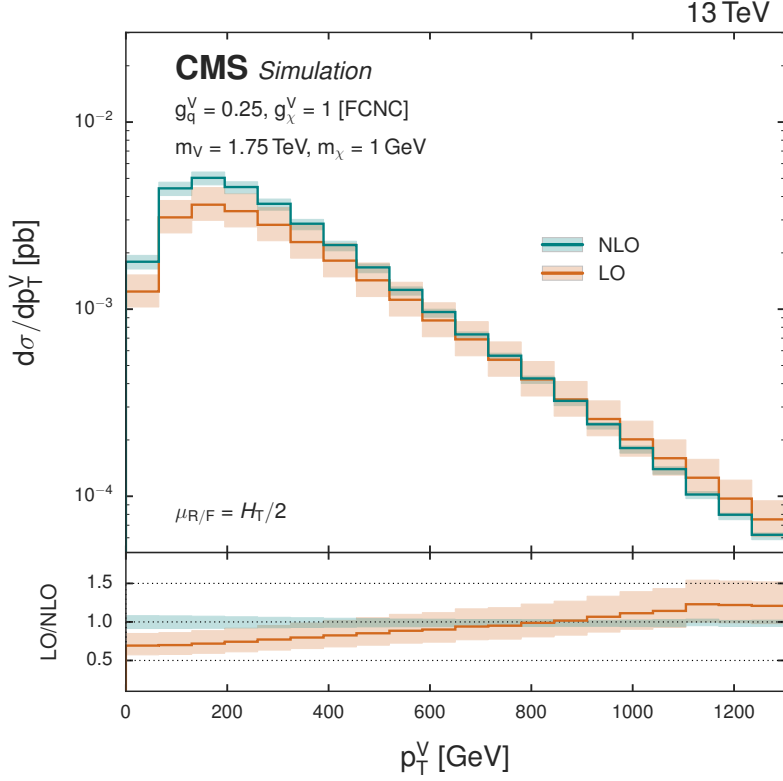


Figure A.1: Inclusive distribution of the transverse momentum of the mediator boson V in the FCNC monotop production mechanism, both at leading-order (LO) and next-to-leading order (NLO) accuracy in QCD, assuming couplings of $g_q^V = 0.25$ and $g_\chi^V = 1$ and masses of 1.75 TeV and 1 GeV for V and the fermionic DM particle χ , respectively. Shaded bands around the central predictions correspond to independent variations of the nominal factorization and renormalization scale $H_T/2$ by factors of 2 and 1/2. While the NLO case exhibits a softer spectrum for p_T^V than the LO computation, which should result in a relatively softer p_T^{miss} , the inclusive cross section increases by about 25% (from 24.8 fb at LO to 31.4 fb at NLO).

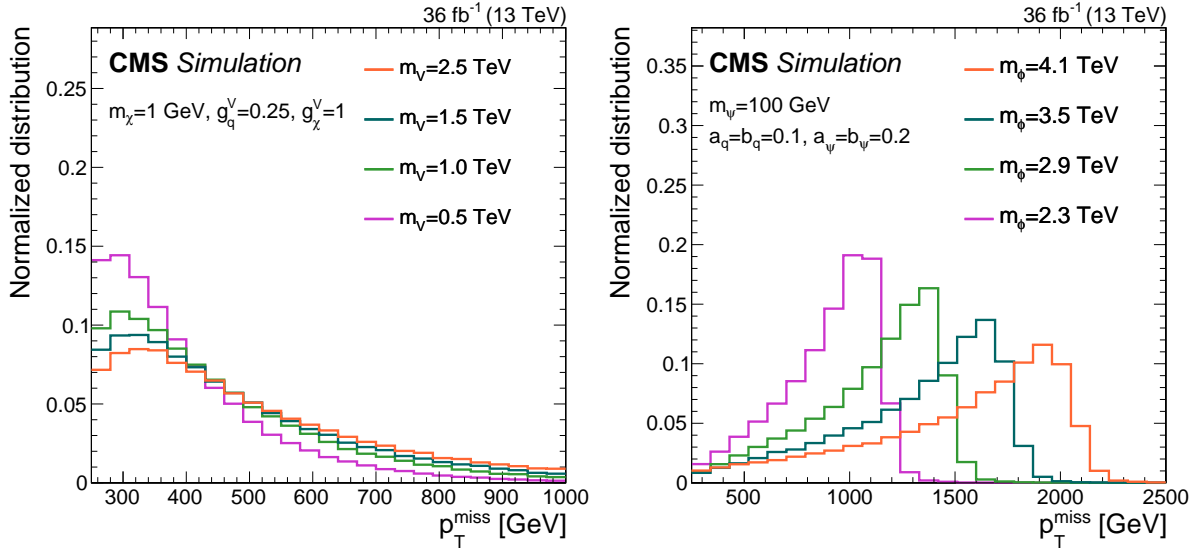


Figure A.2: Distribution of p_T^{miss} in monotop signal models. On the left is shown the FCNC model for various values of m_V ; on the right is the scalar resonance model for various values of m_ϕ

Table A.1: Importance of groups of systematic uncertainties, as measured by the sensitivity of this search to a benchmark FCNC model ($m_V = 2.25 \text{ TeV}$, $m_\chi = 1 \text{ GeV}$). The importance is assessed by evaluating the relative change of the expected 95% CL limit after removing each group of uncertainties. “Other sources” includes all uncertainties not considered elsewhere in the table.

Sources of uncertainty	Change in expected limit (%)
Statistical uncertainty in simulation	3.6
CA15 subjet b tagging	1.4
V+jets renorm./fact. scales and PDF	1.1
Lepton identification	0.7
V+jets electroweak corrections	0.3
V+HF fraction	0.3
AK4 b tagging	< 0.1
Other sources	0.8

Table A.2: Predicted SM backgrounds and yields in data in each bin of the loose signal region, after performing the fit in the control regions only. “Minor backgrounds” refers to the diboson, single t, and QCD multijet backgrounds. The uncertainties are reported as statistical (driven by the data in the CRs), followed by systematic.

p_T^{miss} [GeV]	Z+jets	t \bar{t}	W+jets	Minor backgrounds	Observed	Total backgrounds
250–280	$269.8 \pm 5.6 \pm 18.0$	$148.8 \pm 7.1 \pm 7.9$	$170.3 \pm 3.6 \pm 17.6$	$21.0 \pm 0.3 \pm 4.1$	673	$609.9 \pm 9.8 \pm 26.7$
280–310	$226.1 \pm 5.3 \pm 15.0$	$98.5 \pm 5.3 \pm 7.3$	$127.2 \pm 3.0 \pm 12.9$	$20.2 \pm 0.3 \pm 3.9$	482	$471.9 \pm 8.1 \pm 21.5$
310–350	$178.4 \pm 4.5 \pm 12.9$	$69.1 \pm 4.5 \pm 5.3$	$88.2 \pm 2.2 \pm 8.9$	$14.5 \pm 0.2 \pm 2.8$	358	$350.2 \pm 6.8 \pm 16.8$
350–400	$111.9 \pm 3.3 \pm 8.3$	$32.4 \pm 3.2 \pm 3.0$	$47.1 \pm 1.4 \pm 5.8$	$7.9 \pm 0.1 \pm 1.5$	225	$199.3 \pm 4.8 \pm 10.7$
400–450	$55.3 \pm 2.3 \pm 4.4$	$13.8 \pm 1.7 \pm 2.1$	$17.6 \pm 0.7 \pm 2.3$	$2.6 \pm 0.0 \pm 0.5$	107	$89.4 \pm 2.9 \pm 5.4$
450–600	$57.9 \pm 2.6 \pm 4.2$	$7.6 \pm 1.3 \pm 1.5$	$18.1 \pm 0.8 \pm 2.0$	$3.5 \pm 0.1 \pm 0.7$	100	$87.2 \pm 3.0 \pm 4.9$
600–1000	$12.0 \pm 1.0 \pm 1.2$	$2.2 \pm 0.9 \pm 0.8$	$2.6 \pm 0.2 \pm 0.4$	$1.4 \pm 0.0 \pm 0.3$	19	$18.3 \pm 1.4 \pm 1.5$

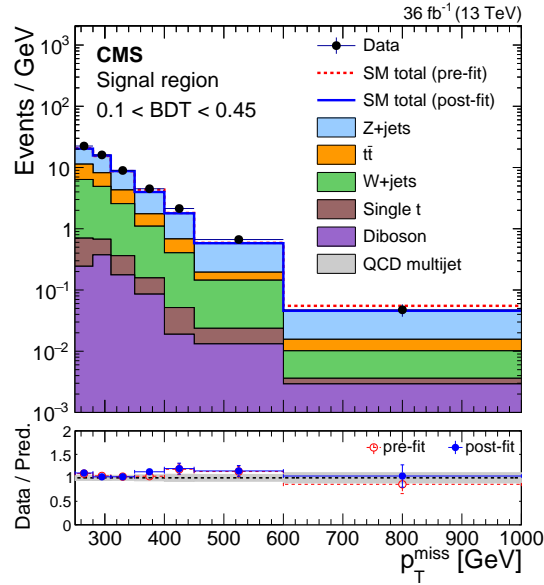


Figure A.3: Distribution of p_T^{miss} from SM backgrounds and data in the loose category of the signal region after fitting the control regions only. Each bin shows the event yields divided by the width of the bin. The stacked histograms show the individual SM background distributions after the fit is performed. The lower panel of the figure shows the ratio of data to fitted prediction. The gray band on the ratio indicates the one standard deviation uncertainty on the prediction after propagating all the systematic uncertainties and their correlations in the fit.

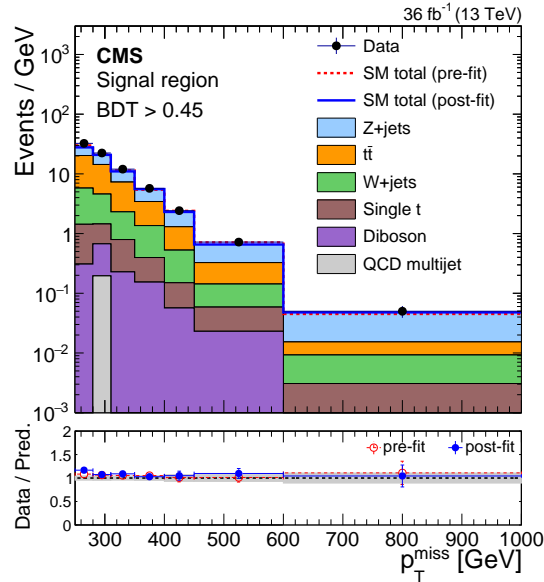


Figure A.4: Distribution of p_T^{miss} from SM backgrounds and data in the tight category of the signal region after fitting the control regions only. Each bin shows the event yields divided by the width of the bin. The stacked histograms show the individual SM background distributions after the fit is performed. The lower panel of the figure shows the ratio of data to fitted prediction. The gray band on the ratio indicates the one standard deviation uncertainty on the prediction after propagating all the systematic uncertainties and their correlations in the fit.

Table A.3: Predicted SM backgrounds and yields in data in each bin of the tight signal region, after performing the fit in the control regions only. “Minor backgrounds” refers to the diboson, single t, and QCD multijet backgrounds. The uncertainties are reported as statistical (driven by the data in the CRs), followed by systematic.

p_T^{miss} [GeV]	Z+jets	$t\bar{t}$	W+jets	Minor backgrounds	Observed	Total backgrounds
250–280	$224.4 \pm 5.7 \pm 16.9$	$435.9 \pm 10.5 \pm 18.8$	$130.4 \pm 3.3 \pm 15.1$	$42.9 \pm 0.8 \pm 9.1$	972	$833.6 \pm 12.4 \pm 30.9$
280–310	$193.4 \pm 5.8 \pm 16.0$	$293.5 \pm 8.6 \pm 13.7$	$94.2 \pm 2.8 \pm 11.5$	$37.6 \pm 0.6 \pm 7.2$	671	$618.6 \pm 10.8 \pm 25.0$
310–350	$149.2 \pm 4.0 \pm 11.0$	$199.1 \pm 6.8 \pm 9.7$	$60.6 \pm 1.6 \pm 7.2$	$31.7 \pm 0.5 \pm 6.4$	480	$440.6 \pm 8.1 \pm 17.6$
350–400	$106.1 \pm 4.0 \pm 8.1$	$104.1 \pm 4.6 \pm 5.3$	$48.2 \pm 1.8 \pm 5.7$	$19.9 \pm 0.3 \pm 3.8$	286	$278.2 \pm 6.3 \pm 11.9$
400–450	$50.2 \pm 2.5 \pm 4.8$	$38.6 \pm 2.6 \pm 3.5$	$18.9 \pm 0.9 \pm 2.7$	$7.5 \pm 0.1 \pm 1.4$	121	$115.2 \pm 3.7 \pm 6.7$
450–600	$49.5 \pm 2.4 \pm 4.8$	$27.5 \pm 2.1 \pm 2.8$	$12.6 \pm 0.6 \pm 1.9$	$8.8 \pm 0.1 \pm 1.7$	108	$98.5 \pm 3.3 \pm 6.1$
600–1000	$13.0 \pm 1.3 \pm 1.1$	$2.4 \pm 0.5 \pm 0.7$	$2.5 \pm 0.2 \pm 0.3$	$1.2 \pm 0.0 \pm 0.3$	20	$19.2 \pm 1.4 \pm 1.4$

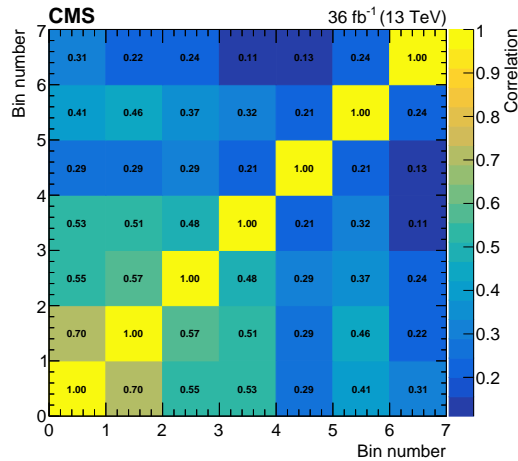


Figure A.5: Correlations between background predictions in each of the bins of the loose signal region, after performing the fit in only the control regions.

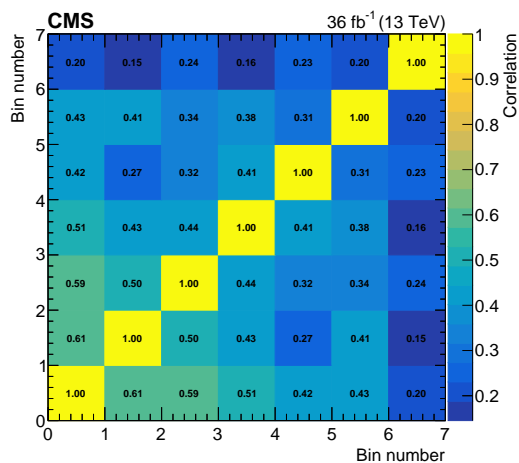


Figure A.6: Correlations between background predictions in each of the bins of the tight signal region, after performing the fit in only the control regions.

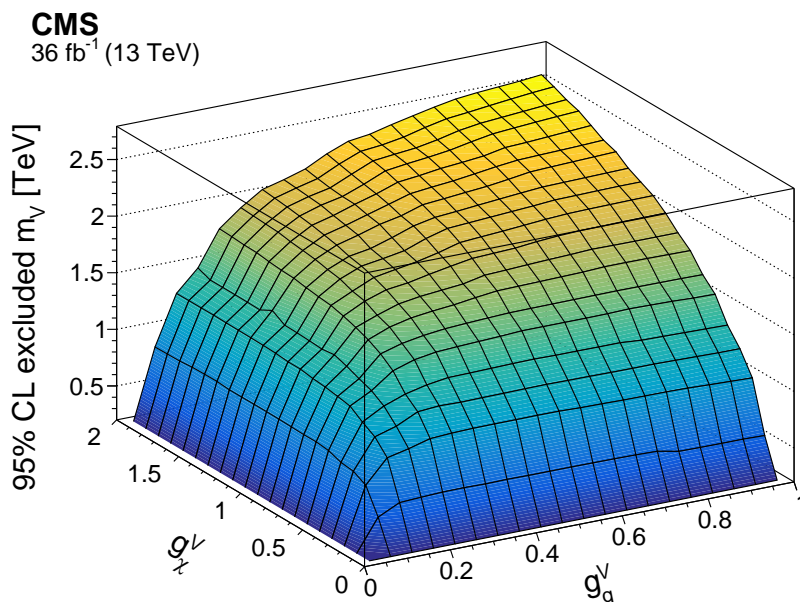


Figure A.7: The maximum excluded mediator mass at 95% CL as a function of vector couplings to DM and quarks. This plot fixes $m_\chi = 1 \text{ GeV}$ and $g_\chi^A = g_q^A = 0$. Masses up to 2.5 TeV are excluded given sufficiently large coupling choices.

B The CMS Collaboration

Yerevan Physics Institute, Yerevan, Armenia

A.M. Sirunyan, A. Tumasyan

Institut für Hochenergiephysik, Wien, Austria

W. Adam, F. Ambrogio, E. Asilar, T. Bergauer, J. Brandstetter, E. Brondolin, M. Dragicevic, J. Erö, M. Flechl, M. Friedl, R. Frühwirth¹, V.M. Ghete, J. Grossmann, J. Hrubec, M. Jeitler¹, A. König, N. Krammer, I. Krätschmer, D. Liko, T. Madlener, I. Mikulec, E. Pree, N. Rad, H. Rohringer, J. Schieck¹, R. Schöfbeck, M. Spanring, D. Spitzbart, W. Waltenberger, J. Wittmann, C.-E. Wulz¹, M. Zarucki

Institute for Nuclear Problems, Minsk, Belarus

V. Chekhovsky, V. Mossolov, J. Suarez Gonzalez

Universiteit Antwerpen, Antwerpen, Belgium

E.A. De Wolf, D. Di Croce, X. Janssen, J. Lauwers, M. Van De Klundert, H. Van Haeuvermaet, P. Van Mechelen, N. Van Remortel

Vrije Universiteit Brussel, Brussel, Belgium

S. Abu Zeid, F. Blekman, J. D'Hondt, I. De Bruyn, J. De Clercq, K. Deroover, G. Flouris, D. Lontkovskyi, S. Lowette, I. Marchesini, S. Moortgat, L. Moreels, Q. Python, K. Skovpen, S. Tavernier, W. Van Doninck, P. Van Mulders, I. Van Parijs

Université Libre de Bruxelles, Bruxelles, Belgium

D. Beghin, H. Brun, B. Clerbaux, G. De Lentdecker, H. Delannoy, B. Dorney, G. Fasanella, L. Favart, R. Goldouzian, A. Grebenyuk, G. Karapostoli, T. Lenzi, J. Luetic, T. Maerschalk, A. Marinov, T. Seva, E. Starling, C. Vander Velde, P. Vanlaer, D. Vannerom, R. Yonamine, F. Zenoni, F. Zhang²

Ghent University, Ghent, Belgium

A. Cimmino, T. Cornelis, D. Dobur, A. Fagot, M. Gul, I. Khvastunov³, D. Poyraz, C. Roskas, S. Salva, M. Tytgat, W. Verbeke, N. Zaganidis

Université Catholique de Louvain, Louvain-la-Neuve, Belgium

H. Bakhshiansohi, O. Bondu, S. Brochet, G. Bruno, C. Caputo, A. Caudron, P. David, S. De Visscher, C. Delaere, M. Delcourt, B. Francois, A. Giammanco, M. Komm, G. Krintiras, V. Lemaitre, A. Magitteri, A. Mertens, M. Musich, K. Piotrkowski, L. Quertenmont, A. Saggio, M. Vidal Marono, S. Wertz, J. Zobec

Université de Mons, Mons, Belgium

N. Beliy

Centro Brasileiro de Pesquisas Fisicas, Rio de Janeiro, Brazil

W.L. Aldá Júnior, F.L. Alves, G.A. Alves, L. Brito, M. Correa Martins Junior, C. Hensel, A. Moraes, M.E. Pol, P. Rebello Teles

Universidade do Estado do Rio de Janeiro, Rio de Janeiro, Brazil

E. Belchior Batista Das Chagas, W. Carvalho, J. Chinellato⁴, E. Coelho, E.M. Da Costa, G.G. Da Silveira⁵, D. De Jesus Damiao, S. Fonseca De Souza, L.M. Huertas Guativa, H. Malbouisson, M. Melo De Almeida, C. Mora Herrera, L. Mundim, H. Nogima, L.J. Sanchez Rosas, A. Santoro, A. Sznajder, M. Thiel, E.J. Tonelli Manganote⁴, F. Torres Da Silva De Araujo, A. Vilela Pereira

Universidade Estadual Paulista ^a, Universidade Federal do ABC ^b, São Paulo, Brazil

S. Ahuja^a, C.A. Bernardes^a, T.R. Fernandez Perez Tomei^a, E.M. Gregores^b, P.G. Mercadante^b, S.F. Novaes^a, Sandra S. Padula^a, D. Romero Abad^b, J.C. Ruiz Vargas^a

Institute for Nuclear Research and Nuclear Energy, Bulgarian Academy of Sciences, Sofia, Bulgaria

A. Aleksandrov, R. Hadjiiska, P. Iaydjiev, M. Misheva, M. Rodozov, M. Shopova, G. Sultanov

University of Sofia, Sofia, Bulgaria

A. Dimitrov, I. Glushkov, L. Litov, B. Pavlov, P. Petkov

Beihang University, Beijing, China

W. Fang⁶, X. Gao⁶, L. Yuan

Institute of High Energy Physics, Beijing, China

M. Ahmad, J.G. Bian, G.M. Chen, H.S. Chen, M. Chen, Y. Chen, C.H. Jiang, D. Leggat, H. Liao, Z. Liu, F. Romeo, S.M. Shaheen, A. Spiezia, J. Tao, C. Wang, Z. Wang, E. Yazgan, H. Zhang, S. Zhang, J. Zhao

State Key Laboratory of Nuclear Physics and Technology, Peking University, Beijing, China

Y. Ban, G. Chen, Q. Li, S. Liu, Y. Mao, S.J. Qian, D. Wang, Z. Xu

Universidad de Los Andes, Bogota, Colombia

C. Avila, A. Cabrera, C.A. Carrillo Montoya, L.F. Chaparro Sierra, C. Florez, C.F. González Hernández, J.D. Ruiz Alvarez, M.A. Segura Delgado

University of Split, Faculty of Electrical Engineering, Mechanical Engineering and Naval Architecture, Split, Croatia

B. Courbon, N. Godinovic, D. Lelas, I. Puljak, P.M. Ribeiro Cipriano, T. Sculac

University of Split, Faculty of Science, Split, Croatia

Z. Antunovic, M. Kovac

Institute Rudjer Boskovic, Zagreb, Croatia

V. Brigljevic, D. Ferencek, K. Kadija, B. Mesic, A. Starodumov⁷, T. Susa

University of Cyprus, Nicosia, Cyprus

M.W. Ather, A. Attikis, G. Mavromanolakis, J. Mousa, C. Nicolaou, F. Ptochos, P.A. Razis, H. Rykaczewski

Charles University, Prague, Czech Republic

M. Finger⁸, M. Finger Jr.⁸

Universidad San Francisco de Quito, Quito, Ecuador

E. Carrera Jarrin

Academy of Scientific Research and Technology of the Arab Republic of Egypt, Egyptian Network of High Energy Physics, Cairo, Egypt

E. El-khateeb⁹, S. Elgammal¹⁰, A. Mohamed¹¹

National Institute of Chemical Physics and Biophysics, Tallinn, Estonia

R.K. Dewanjee, M. Kadastik, L. Perrini, M. Raidal, A. Tiko, C. Veelken

Department of Physics, University of Helsinki, Helsinki, Finland

P. Eerola, H. Kirschenmann, J. Pekkanen, M. Voutilainen

Helsinki Institute of Physics, Helsinki, Finland

J. Havukainen, J.K. Heikkilä, T. Järvinen, V. Karimäki, R. Kinnunen, T. Lampén, K. Lassila-Perini, S. Laurila, S. Lehti, T. Lindén, P. Luukka, H. Siikonen, E. Tuominen, J. Tuominiemi

Lappeenranta University of Technology, Lappeenranta, Finland

J. Talvitie, T. Tuuva

IRFU, CEA, Université Paris-Saclay, Gif-sur-Yvette, France

M. Besancon, F. Couderc, M. Dejardin, D. Denegri, J.L. Faure, F. Ferri, S. Ganjour, S. Ghosh, A. Givernaud, P. Gras, G. Hamel de Monchenault, P. Jarry, I. Kucher, C. Leloup, E. Locci, M. Machet, J. Malcles, G. Negro, J. Rander, A. Rosowsky, M.Ö. Sahin, M. Titov

Laboratoire Leprince-Ringuet, Ecole polytechnique, CNRS/IN2P3, Université Paris-Saclay, Palaiseau, France

A. Abdulsalam, C. Amendola, I. Antropov, S. Baffioni, F. Beaudette, P. Busson, L. Cadamuro, C. Charlot, R. Granier de Cassagnac, M. Jo, S. Lisniak, A. Lobanov, J. Martin Blanco, M. Nguyen, C. Ochando, G. Ortona, P. Paganini, P. Pigard, R. Salerno, J.B. Sauvan, Y. Sirois, A.G. Stahl Leitner, T. Strebler, Y. Yilmaz, A. Zabi, A. Zghiche

Université de Strasbourg, CNRS, IPHC UMR 7178, F-67000 Strasbourg, France

J.-L. Agram¹², J. Andrea, D. Bloch, J.-M. Brom, M. Buttignol, E.C. Chabert, N. Chanon, C. Collard, E. Conte¹², X. Coubez, J.-C. Fontaine¹², D. Gelé, U. Goerlach, M. Jansová, A.-C. Le Bihan, N. Tonon, P. Van Hove

Centre de Calcul de l'Institut National de Physique Nucleaire et de Physique des Particules, CNRS/IN2P3, Villeurbanne, France

S. Gadrat

Université de Lyon, Université Claude Bernard Lyon 1, CNRS-IN2P3, Institut de Physique Nucléaire de Lyon, Villeurbanne, France

S. Beauceron, C. Bernet, G. Boudoul, R. Chierici, D. Contardo, P. Depasse, H. El Mamouni, J. Fay, L. Finco, S. Gascon, M. Gouzevitch, G. Grenier, B. Ille, F. Lagarde, I.B. Laktineh, M. Lethuillier, L. Mirabito, A.L. Pequegnot, S. Perries, A. Popov¹³, V. Sordini, M. Vander Donckt, S. Viret

Georgian Technical University, Tbilisi, Georgia

A. Khvedelidze⁸

Tbilisi State University, Tbilisi, Georgia

Z. Tsamalaidze⁸

RWTH Aachen University, I. Physikalisches Institut, Aachen, Germany

C. Autermann, L. Feld, M.K. Kiesel, K. Klein, M. Lipinski, M. Preuten, C. Schomakers, J. Schulz, V. Zhukov¹³

RWTH Aachen University, III. Physikalisches Institut A, Aachen, Germany

A. Albert, E. Dietz-Laursonn, D. Duchardt, M. Endres, M. Erdmann, S. Erdweg, T. Esch, R. Fischer, A. Güth, M. Hamer, T. Hebbeker, C. Heidemann, K. Hoepfner, S. Knutzen, M. Merschmeyer, A. Meyer, P. Millet, S. Mukherjee, T. Pook, M. Radziej, H. Reithler, M. Rieger, F. Scheuch, D. Teyssier, S. Thüer

RWTH Aachen University, III. Physikalisches Institut B, Aachen, Germany

G. Flügge, B. Kargoll, T. Kress, A. Künsken, T. Müller, A. Nehr Korn, A. Nowack, C. Pistone, O. Pooth, A. Stahl¹⁴

Deutsches Elektronen-Synchrotron, Hamburg, Germany

M. Aldaya Martin, T. Arndt, C. Asawatangtrakuldee, K. Beernaert, O. Behnke, U. Behrens, A. Bermúdez Martínez, A.A. Bin Anuar, K. Borras¹⁵, V. Botta, A. Campbell, P. Connor, C. Contreras-Campana, F. Costanza, C. Diez Pardos, G. Eckerlin, D. Eckstein, T. Eichhorn, E. Eren, E. Gallo¹⁶, J. Garay Garcia, A. Geiser, A. Gizhko, J.M. Grados Luyando, A. Grohsjean, P. Gunnellini, M. Guthoff, A. Harb, J. Hauk, M. Hempel¹⁷, H. Jung, A. Kalogeropoulos, M. Kasemann, J. Keaveney, C. Kleinwort, I. Korol, D. Krücker, W. Lange, A. Lelek, T. Lenz, J. Leonard, K. Lipka, W. Lohmann¹⁷, R. Mankel, I.-A. Melzer-Pellmann, A.B. Meyer, G. Mittag, J. Mnich, A. Mussgiller, E. Ntomari, D. Pitzl, A. Raspereza, M. Savitskyi, P. Saxena, R. Shevchenko, S. Spannagel, N. Stefaniuk, G.P. Van Onsem, R. Walsh, Y. Wen, K. Wichmann, C. Wissing, O. Zenaiev

University of Hamburg, Hamburg, Germany

R. Aggleton, S. Bein, V. Blobel, M. Centis Vignali, T. Dreyer, E. Garutti, D. Gonzalez, J. Haller, A. Hinzmann, M. Hoffmann, A. Karavdina, R. Klanner, R. Kogler, N. Kovalchuk, S. Kurz, T. Lapsien, D. Marconi, M. Meyer, M. Niedziela, D. Nowatschin, F. Pantaleo¹⁴, T. Peiffer, A. Perieanu, C. Scharf, P. Schleper, A. Schmidt, S. Schumann, J. Schwandt, J. Sonneveld, H. Stadie, G. Steinbrück, F.M. Stober, M. Stöver, H. Tholen, D. Troendle, E. Usai, A. Vanhoefler, B. Vormwald

Institut für Experimentelle Kernphysik, Karlsruhe, Germany

M. Akbiyik, C. Barth, M. Baselga, S. Baur, E. Butz, R. Caspart, T. Chwalek, F. Colombo, W. De Boer, A. Dierlamm, N. Faltermann, B. Freund, R. Friese, M. Giffels, M.A. Harrendorf, F. Hartmann¹⁴, S.M. Heindl, U. Husemann, F. Kassel¹⁴, S. Kudella, H. Mildner, M.U. Mozer, Th. Müller, M. Plagge, G. Quast, K. Rabbertz, M. Schröder, I. Shvetsov, G. Sieber, H.J. Simonis, R. Ulrich, S. Wayand, M. Weber, T. Weiler, S. Williamson, C. Wöhrmann, R. Wolf

Institute of Nuclear and Particle Physics (INPP), NCSR Demokritos, Aghia Paraskevi, Greece

G. Anagnostou, G. Daskalakis, T. Gerasis, A. Kyriakis, D. Loukas, I. Topsis-Giotis

National and Kapodistrian University of Athens, Athens, Greece

G. Karathanasis, S. Kesisoglou, A. Panagiotou, N. Saoulidou

National Technical University of Athens, Athens, Greece

K. Kousouris

University of Ioánnina, Ioánnina, Greece

I. Evangelou, C. Foudas, P. Kokkas, S. Mallios, N. Manthos, I. Papadopoulos, E. Paradas, J. Strologas, F.A. Triantis

MTA-ELTE Lendület CMS Particle and Nuclear Physics Group, Eötvös Loránd University, Budapest, Hungary

M. Csanad, N. Filipovic, G. Pasztor, O. Surányi, G.I. Veres¹⁸

Wigner Research Centre for Physics, Budapest, Hungary

G. Bencze, C. Hajdu, D. Horvath¹⁹, Á. Hunyadi, F. Sikler, V. Veszpremi

Institute of Nuclear Research ATOMKI, Debrecen, Hungary

N. Beni, S. Czellar, J. Karacsi²⁰, A. Makovec, J. Molnar, Z. Szillasi

Institute of Physics, University of Debrecen, Debrecen, Hungary

M. Bartók¹⁸, P. Raics, Z.L. Trocsanyi, B. Ujvari

Indian Institute of Science (IISc), Bangalore, India

S. Choudhury, J.R. Komaragiri

National Institute of Science Education and Research, Bhubaneswar, IndiaS. Bahinipati²¹, S. Bhowmik, P. Mal, K. Mandal, A. Nayak²², D.K. Sahoo²¹, N. Sahoo, S.K. Swain**Panjab University, Chandigarh, India**

S. Bansal, S.B. Beri, V. Bhatnagar, R. Chawla, N. Dhingra, A.K. Kalsi, A. Kaur, M. Kaur, S. Kaur, R. Kumar, P. Kumari, A. Mehta, J.B. Singh, G. Walia

University of Delhi, Delhi, India

A. Bhardwaj, S. Chauhan, B.C. Choudhary, R.B. Garg, S. Keshri, A. Kumar, Ashok Kumar, S. Malhotra, M. Naimuddin, K. Ranjan, Aashaq Shah, R. Sharma

Saha Institute of Nuclear Physics, HBNI, Kolkata, India

R. Bhardwaj, R. Bhattacharya, S. Bhattacharya, U. Bhawandeep, S. Dey, S. Dutt, S. Dutta, S. Ghosh, N. Majumdar, A. Modak, K. Mondal, S. Mukhopadhyay, S. Nandan, A. Purohit, A. Roy, S. Roy Chowdhury, S. Sarkar, M. Sharan, S. Thakur

Indian Institute of Technology Madras, Madras, India

P.K. Behera

Bhabha Atomic Research Centre, Mumbai, IndiaR. Chudasama, D. Dutta, V. Jha, V. Kumar, A.K. Mohanty¹⁴, P.K. Netrakanti, L.M. Pant, P. Shukla, A. Topkar**Tata Institute of Fundamental Research-A, Mumbai, India**

T. Aziz, S. Dugad, B. Mahakud, S. Mitra, G.B. Mohanty, N. Sur, B. Sutar

Tata Institute of Fundamental Research-B, Mumbai, IndiaS. Banerjee, S. Bhattacharya, S. Chatterjee, P. Das, M. Guchait, Sa. Jain, S. Kumar, M. Maity²³, G. Majumder, K. Mazumdar, T. Sarkar²³, N. Wickramage²⁴**Indian Institute of Science Education and Research (IISER), Pune, India**

S. Chauhan, S. Dube, V. Hegde, A. Kapoor, K. Kothekar, S. Pandey, A. Rane, S. Sharma

Institute for Research in Fundamental Sciences (IPM), Tehran, IranS. Chenarani²⁵, E. Eskandari Tadavani, S.M. Etesami²⁵, M. Khakzad, M. Mohammadi Najafabadi, M. Naseri, S. Paktinat Mehdiabadi²⁶, F. Rezaei Hosseinabadi, B. Safarzadeh²⁷, M. Zeinali**University College Dublin, Dublin, Ireland**

M. Felcini, M. Grunewald

INFN Sezione di Bari ^a, Università di Bari ^b, Politecnico di Bari ^c, Bari, ItalyM. Abbrescia^{a,b}, C. Calabria^{a,b}, A. Colaleo^a, D. Creanza^{a,c}, L. Cristella^{a,b}, N. De Filippis^{a,c}, M. De Palma^{a,b}, F. Errico^{a,b}, L. Fiore^a, G. Iaselli^{a,c}, S. Lezki^{a,b}, G. Maggi^{a,c}, M. Maggi^a, G. Miniello^{a,b}, S. My^{a,b}, S. Nuzzo^{a,b}, A. Pompili^{a,b}, G. Pugliese^{a,c}, R. Radogna^a, A. Ranieri^a, G. Selvaggi^{a,b}, A. Sharma^a, L. Silvestris^{a,14}, R. Venditti^a, P. Verwilligen^a**INFN Sezione di Bologna ^a, Università di Bologna ^b, Bologna, Italy**G. Abbiendi^a, C. Battilana^{a,b}, D. Bonacorsi^{a,b}, L. Borgonovi^{a,b}, S. Braibant-Giacomelli^{a,b}, R. Campanini^{a,b}, P. Capiluppi^{a,b}, A. Castro^{a,b}, F.R. Cavallo^a, S.S. Chhibra^a, G. Codispoti^{a,b}, M. Cuffiani^{a,b}, G.M. Dallavalle^a, F. Fabbri^a, A. Fanfani^{a,b}, D. Fasanella^{a,b}, P. Giacomelli^a, C. Grandi^a, L. Guiducci^{a,b}, S. Marcellini^a, G. Masetti^a, A. Montanari^a, F.L. Navarria^{a,b}, A. Perrotta^a, A.M. Rossi^{a,b}, T. Rovelli^{a,b}, G.P. Siroli^{a,b}, N. Tosi^a

INFN Sezione di Catania ^a, Università di Catania ^b, Catania, Italy

S. Albergo^{a,b}, S. Costa^{a,b}, A. Di Mattia^a, F. Giordano^{a,b}, R. Potenza^{a,b}, A. Tricomi^{a,b}, C. Tuve^{a,b}

INFN Sezione di Firenze ^a, Università di Firenze ^b, Firenze, Italy

G. Barbagli^a, K. Chatterjee^{a,b}, V. Ciulli^{a,b}, C. Civinini^a, R. D'Alessandro^{a,b}, E. Focardi^{a,b}, P. Lenzi^{a,b}, M. Meschini^a, S. Paoletti^a, L. Russo^{a,28}, G. Sguazzoni^a, D. Strom^a, L. Viliani^{a,b,14}

INFN Laboratori Nazionali di Frascati, Frascati, Italy

L. Benussi, S. Bianco, F. Fabbri, D. Piccolo, F. Primavera¹⁴

INFN Sezione di Genova ^a, Università di Genova ^b, Genova, Italy

V. Calvelli^{a,b}, F. Ferro^a, E. Robutti^a, S. Tosi^{a,b}

INFN Sezione di Milano-Bicocca ^a, Università di Milano-Bicocca ^b, Milano, Italy

A. Benaglia^a, A. Beschi^b, L. Brianza^{a,b}, F. Brivio^{a,b}, V. Ciriolo^{a,b,14}, M.E. Dinardo^{a,b}, S. Fiorendi^{a,b}, S. Gennai^a, A. Ghezzi^{a,b}, P. Govoni^{a,b}, M. Malberti^{a,b}, S. Malvezzi^a, R.A. Manzoni^{a,b}, D. Menasce^a, L. Moroni^a, M. Paganoni^{a,b}, K. Pauwels^{a,b}, D. Pedrini^a, S. Pigazzini^{a,b,29}, S. Ragazzi^{a,b}, T. Tabarelli de Fatis^{a,b}

INFN Sezione di Napoli ^a, Università di Napoli 'Federico II' ^b, Napoli, Italy, Università della Basilicata ^c, Potenza, Italy, Università G. Marconi ^d, Roma, Italy

S. Buontempo^a, N. Cavallo^{a,c}, S. Di Guida^{a,d,14}, F. Fabozzi^{a,c}, F. Fienga^{a,b}, A.O.M. Iorio^{a,b}, W.A. Khan^a, L. Lista^a, S. Meola^{a,d,14}, P. Paolucci^{a,14}, C. Sciacca^{a,b}, F. Thyssen^a

INFN Sezione di Padova ^a, Università di Padova ^b, Padova, Italy, Università di Trento ^c, Trento, Italy

P. Azzi^a, N. Bacchetta^a, L. Benato^{a,b}, D. Bisello^{a,b}, A. Boletti^{a,b}, R. Carlin^{a,b}, A. Carvalho Antunes De Oliveira^{a,b}, P. Checchia^a, M. Dall'Osso^{a,b}, P. De Castro Manzano^a, T. Dorigo^a, U. Dosselli^a, F. Gasparini^{a,b}, U. Gasparini^{a,b}, A. Gozzelino^a, S. Lacaprara^a, P. Lujan, M. Margoni^{a,b}, A.T. Meneguzzo^{a,b}, N. Pozzobon^{a,b}, P. Ronchese^{a,b}, R. Rossin^{a,b}, F. Simonetto^{a,b}, E. Torassa^a, M. Zanetti^{a,b}, P. Zotto^{a,b}

INFN Sezione di Pavia ^a, Università di Pavia ^b, Pavia, Italy

A. Braghieri^a, A. Magnani^a, P. Montagna^{a,b}, S.P. Ratti^{a,b}, V. Re^a, M. Ressegotti^{a,b}, C. Riccardi^{a,b}, P. Salvini^a, I. Vai^{a,b}, P. Vitulo^{a,b}

INFN Sezione di Perugia ^a, Università di Perugia ^b, Perugia, Italy

L. Alunni Solestizi^{a,b}, M. Biasini^{a,b}, G.M. Bilei^a, C. Cecchi^{a,b}, D. Ciangottini^{a,b}, L. Fanò^{a,b}, P. Lariccia^{a,b}, R. Leonardi^{a,b}, E. Manoni^a, G. Mantovani^{a,b}, V. Mariani^{a,b}, M. Menichelli^a, A. Rossi^{a,b}, A. Santocchia^{a,b}, D. Spiga^a

INFN Sezione di Pisa ^a, Università di Pisa ^b, Scuola Normale Superiore di Pisa ^c, Pisa, Italy

K. Androsov^a, P. Azzurri^{a,14}, G. Bagliesi^a, T. Boccali^a, L. Borrello, R. Castaldi^a, M.A. Ciocci^{a,b}, R. Dell'Orso^a, G. Fedia^a, L. Giannini^{a,c}, A. Giassi^a, M.T. Grippo^{a,28}, F. Ligabue^{a,c}, T. Lomtadze^a, E. Manca^{a,c}, G. Mandorli^{a,c}, A. Messineo^{a,b}, F. Palla^a, A. Rizzi^{a,b}, A. Savoy-Navarro^{a,30}, P. Spagnolo^a, R. Tenchini^a, G. Tonelli^{a,b}, A. Venturi^a, P.G. Verdini^a

INFN Sezione di Roma ^a, Sapienza Università di Roma ^b, Rome, Italy

L. Barone^{a,b}, F. Cavallari^a, M. Cipriani^{a,b}, N. Daci^a, D. Del Re^{a,b,14}, E. Di Marco^{a,b}, M. Diemoz^a, S. Gelli^{a,b}, E. Longo^{a,b}, F. Margaroli^{a,b}, B. Marzocchi^{a,b}, P. Meridiani^a, G. Organtini^{a,b}, R. Paramatti^{a,b}, F. Preiato^{a,b}, S. Rahatlou^{a,b}, C. Rovelli^a, F. Santanastasio^{a,b}

INFN Sezione di Torino ^a, Università di Torino ^b, Torino, Italy, Università del Piemonte Orientale ^c, Novara, Italy

N. Amapane^{a,b}, R. Arcidiacono^{a,c}, S. Argiro^{a,b}, M. Arneodo^{a,c}, N. Bartosik^a, R. Bellan^{a,b},

C. Biino^a, N. Cartiglia^a, F. Cenna^{a,b}, M. Costa^{a,b}, R. Covarelli^{a,b}, A. Degano^{a,b}, N. Demaria^a, B. Kiani^{a,b}, C. Mariotti^a, S. Maselli^a, E. Migliore^{a,b}, V. Monaco^{a,b}, E. Monteil^{a,b}, M. Monteno^a, M.M. Obertino^{a,b}, L. Pacher^{a,b}, N. Pastrone^a, M. Pelliccioni^a, G.L. Pinna Angioni^{a,b}, F. Ravera^{a,b}, A. Romero^{a,b}, M. Ruspa^{a,c}, R. Sacchi^{a,b}, K. Shchelina^{a,b}, V. Sola^a, A. Solano^{a,b}, A. Staiano^a, P. Traczyk^{a,b}

INFN Sezione di Trieste^a, Università di Trieste^b, Trieste, Italy
S. Belforte^a, M. Casarsa^a, F. Cossutti^a, G. Della Ricca^{a,b}, A. Zanetti^a

Kyungpook National University, Daegu, Korea

D.H. Kim, G.N. Kim, M.S. Kim, J. Lee, S. Lee, S.W. Lee, C.S. Moon, Y.D. Oh, S. Sekmen, D.C. Son, Y.C. Yang

Chonbuk National University, Jeonju, Korea

A. Lee

Chonnam National University, Institute for Universe and Elementary Particles, Kwangju, Korea

H. Kim, D.H. Moon, G. Oh

Hanyang University, Seoul, Korea

J.A. Brochero Cifuentes, J. Goh, T.J. Kim

Korea University, Seoul, Korea

S. Cho, S. Choi, Y. Go, D. Gyun, S. Ha, B. Hong, Y. Jo, Y. Kim, K. Lee, K.S. Lee, S. Lee, J. Lim, S.K. Park, Y. Roh

Seoul National University, Seoul, Korea

J. Almond, J. Kim, J.S. Kim, H. Lee, K. Lee, K. Nam, S.B. Oh, B.C. Radburn-Smith, S.h. Seo, U.K. Yang, H.D. Yoo, G.B. Yu

University of Seoul, Seoul, Korea

M. Choi, H. Kim, J.H. Kim, J.S.H. Lee, I.C. Park

Sungkyunkwan University, Suwon, Korea

Y. Choi, C. Hwang, J. Lee, I. Yu

Vilnius University, Vilnius, Lithuania

V. Dudenas, A. Juodagalvis, J. Vaitkus

National Centre for Particle Physics, Universiti Malaya, Kuala Lumpur, Malaysia

I. Ahmed, Z.A. Ibrahim, M.A.B. Md Ali³¹, F. Mohamad Idris³², W.A.T. Wan Abdullah, M.N. Yusli, Z. Zolkapli

Centro de Investigacion y de Estudios Avanzados del IPN, Mexico City, Mexico

Duran-Osuna, M. C., H. Castilla-Valdez, E. De La Cruz-Burelo, Ramirez-Sanchez, G., I. Heredia-De La Cruz³³, Rabadan-Trejo, R. I., R. Lopez-Fernandez, J. Mejia Guisao, Reyes-Almanza, R, A. Sanchez-Hernandez

Universidad Iberoamericana, Mexico City, Mexico

S. Carrillo Moreno, C. Oropeza Barrera, F. Vazquez Valencia

Benemerita Universidad Autonoma de Puebla, Puebla, Mexico

I. Pedraza, H.A. Salazar Ibarguen, C. Uribe Estrada

Universidad Autónoma de San Luis Potosí, San Luis Potosí, Mexico

A. Morelos Pineda

University of Auckland, Auckland, New Zealand

D. Krofcheck

University of Canterbury, Christchurch, New Zealand

P.H. Butler

National Centre for Physics, Quaid-I-Azam University, Islamabad, Pakistan

A. Ahmad, M. Ahmad, Q. Hassan, H.R. Hoorani, A. Saddique, M.A. Shah, M. Shoaib, M. Waqas

National Centre for Nuclear Research, Swierk, Poland

H. Bialkowska, M. Bluj, B. Boimska, T. Frueboes, M. Górski, M. Kazana, K. Nawrocki, M. Szleper, P. Zalewski

Institute of Experimental Physics, Faculty of Physics, University of Warsaw, Warsaw, PolandK. Bunkowski, A. Byszuk³⁴, K. Doroba, A. Kalinowski, M. Konecki, J. Krolikowski, M. Misiura, M. Olszewski, A. Pyskir, M. Walczak**Laboratório de Instrumentação e Física Experimental de Partículas, Lisboa, Portugal**

P. Bargassa, C. Beirão Da Cruz E Silva, A. Di Francesco, P. Faccioli, B. Galinhas, M. Gallinaro, J. Hollar, N. Leonardo, L. Lloret Iglesias, M.V. Nemallapudi, J. Seixas, G. Strong, O. Toldaiev, D. Vadrucio, J. Varela

Joint Institute for Nuclear Research, Dubna, RussiaV. Alexakhin, P. Bunin, M. Gavrilenko, A. Golunov, I. Golutvin, N. Gorbounov, I. Gorbunov, V. Karjavin, A. Lanev, A. Malakhov, V. Matveev^{35,36}, V. Palichik, V. Perelygin, M. Savina, S. Shmatov, S. Shulha, V. Smirnov, A. Zarubin**Petersburg Nuclear Physics Institute, Gatchina (St. Petersburg), Russia**Y. Ivanov, V. Kim³⁷, E. Kuznetsova³⁸, P. Levchenko, V. Murzin, V. Oreshkin, I. Smirnov, V. Sulimov, L. Uvarov, S. Vavilov, A. Vorobyev**Institute for Nuclear Research, Moscow, Russia**

Yu. Andreev, A. Dermenev, S. Gninenko, N. Golubev, A. Karneyeu, M. Kirsanov, N. Krasnikov, A. Pashenkov, D. Tlisov, A. Toropin

Institute for Theoretical and Experimental Physics, Moscow, Russia

V. Epshteyn, V. Gavrilov, N. Lychkovskaya, V. Popov, I. Pozdnyakov, G. Safronov, A. Spiridonov, A. Stepenov, M. Toms, E. Vlasov, A. Zhokin

Moscow Institute of Physics and Technology, Moscow, RussiaT. Aushev, A. Bylinkin³⁶**National Research Nuclear University 'Moscow Engineering Physics Institute' (MEPhI), Moscow, Russia**R. Chistov³⁹, M. Danilov³⁹, P. Parygin, D. Philippov, S. Polikarpov, E. Tarkovskii**P.N. Lebedev Physical Institute, Moscow, Russia**V. Andreev, M. Azarkin³⁶, I. Dremin³⁶, M. Kirakosyan³⁶, A. Terkulov**Skobeltsyn Institute of Nuclear Physics, Lomonosov Moscow State University, Moscow, Russia**A. Baskakov, A. Belyaev, E. Boos, V. Bunichev, M. Dubinin⁴⁰, L. Dudko, A. Ershov, V. Klyukhin, N. Korneeva, I. Lokhtin, I. Miagkov, S. Obraztsov, M. Perfilov, V. Savrin, P. Volkov**Novosibirsk State University (NSU), Novosibirsk, Russia**V. Blinov⁴¹, D. Shtol⁴¹, Y. Skovpen⁴¹

State Research Center of Russian Federation, Institute for High Energy Physics of NRC ", Kurchatov Institute", , Protvino, Russia

I. Azhgirey, I. Bayshev, S. Bitioukov, D. Elumakhov, V. Kachanov, A. Kalinin, D. Konstantinov, P. Mandrik, V. Petrov, R. Ryutin, A. Sobol, S. Troshin, N. Tyurin, A. Uzunian, A. Volkov

University of Belgrade, Faculty of Physics and Vinca Institute of Nuclear Sciences, Belgrade, Serbia

P. Adzic⁴², P. Cirkovic, D. Devetak, M. Dordevic, J. Milosevic, V. Rekovic

Centro de Investigaciones Energéticas Medioambientales y Tecnológicas (CIEMAT), Madrid, Spain

J. Alcaraz Maestre, A. Álvarez Fernández, M. Barrio Luna, M. Cerrada, N. Colino, B. De La Cruz, A. Delgado Peris, A. Escalante Del Valle, C. Fernandez Bedoya, J.P. Fernández Ramos, J. Flix, M.C. Fouz, O. Gonzalez Lopez, S. Goy Lopez, J.M. Hernandez, M.I. Josa, D. Moran, A. Pérez-Calero Yzquierdo, J. Puerta Pelayo, A. Quintario Olmeda, I. Redondo, L. Romero, M.S. Soares

Universidad Autónoma de Madrid, Madrid, Spain

C. Albajar, J.F. de Trocóniz, M. Missiroli

Universidad de Oviedo, Oviedo, Spain

J. Cuevas, C. Erice, J. Fernandez Menendez, I. Gonzalez Caballero, J.R. González Fernández, E. Palencia Cortezon, S. Sanchez Cruz, P. Vischia, J.M. Vizan Garcia

Instituto de Física de Cantabria (IFCA), CSIC-Universidad de Cantabria, Santander, Spain

I.J. Cabrillo, A. Calderon, B. Chazin Quero, E. Curras, J. Duarte Campderros, M. Fernandez, J. Garcia-Ferrero, G. Gomez, A. Lopez Virto, J. Marco, C. Martinez Rivero, P. Martinez Ruiz del Arbol, F. Matorras, J. Piedra Gomez, T. Rodrigo, A. Ruiz-Jimeno, L. Scodellaro, N. Trevisani, I. Vila, R. Vilar Cortabitarte

CERN, European Organization for Nuclear Research, Geneva, Switzerland

D. Abbaneo, B. Akgun, E. Auffray, P. Baillon, A.H. Ball, D. Barney, J. Bendavid, M. Bianco, P. Bloch, A. Bocci, C. Botta, T. Camporesi, R. Castello, M. Cepeda, G. Cerminara, E. Chapon, Y. Chen, D. d'Enterria, A. Dabrowski, V. Daponte, A. David, M. De Gruttola, A. De Roeck, N. Deelen, M. Dobson, T. du Pree, M. Dünser, N. Dupont, A. Elliott-Peisert, P. Everaerts, F. Fallavollita, G. Franzoni, J. Fulcher, W. Funk, D. Gigi, A. Gilbert, K. Gill, F. Glege, D. Gulhan, P. Harris, J. Hegeman, V. Innocente, A. Jafari, P. Janot, O. Karacheban¹⁷, J. Kieseler, V. Knünz, A. Kornmayer, M.J. Kortelainen, M. Krammer¹, C. Lange, P. Lecoq, C. Lourenço, M.T. Lucchini, L. Malgeri, M. Mannelli, A. Martelli, F. Meijers, J.A. Merlin, S. Mersi, E. Meschi, P. Milenovic⁴³, F. Moortgat, M. Mulders, H. Neugebauer, J. Ngadiuba, S. Orfanelli, L. Orsini, L. Pape, E. Perez, M. Peruzzi, A. Petrilli, G. Petrucciani, A. Pfeiffer, M. Pierini, D. Rabady, A. Racz, T. Reis, G. Rolandi⁴⁴, M. Rovere, H. Sakulin, C. Schäfer, C. Schwick, M. Seidel, M. Selvaggi, A. Sharma, P. Silva, P. Sphicas⁴⁵, A. Stakia, J. Steggemann, M. Stoye, M. Tosi, D. Treille, A. Triossi, A. Tsirou, V. Veckalns⁴⁶, M. Verweij, W.D. Zeuner

Paul Scherrer Institut, Villigen, Switzerland

W. Bertl[†], L. Caminada⁴⁷, K. Deiters, W. Erdmann, R. Horisberger, Q. Ingram, H.C. Kaestli, D. Kotlinski, U. Langenegger, T. Rohe, S.A. Wiederkehr

ETH Zurich - Institute for Particle Physics and Astrophysics (IPA), Zurich, Switzerland

M. Backhaus, L. Bäni, P. Berger, L. Bianchini, B. Casal, G. Dissertori, M. Dittmar, M. Donegà, C. Dorfer, C. Grab, C. Heidegger, D. Hits, J. Hoss, G. Kasieczka, T. Klijsma, W. Lustermann,

B. Mangano, M. Marionneau, M.T. Meinhard, D. Meister, F. Micheli, P. Musella, F. Nessi-Tedaldi, F. Pandolfi, J. Pata, F. Pauss, G. Perrin, L. Perrozzi, M. Quittnat, M. Reichmann, D.A. Sanz Becerra, M. Schönenberger, L. Shchutska, V.R. Tavolaro, K. Theofilatos, M.L. Vesterbacka Olsson, R. Wallny, D.H. Zhu

Universität Zürich, Zurich, Switzerland

T.K. Aarrestad, C. Amsler⁴⁸, M.F. Canelli, A. De Cosa, R. Del Burgo, S. Donato, C. Galloni, T. Hreus, B. Kilminster, D. Pinna, G. Rauco, P. Robmann, D. Salerno, K. Schweiger, C. Seitz, Y. Takahashi, A. Zucchetta

National Central University, Chung-Li, Taiwan

V. Candelise, T.H. Doan, Sh. Jain, R. Khurana, C.M. Kuo, W. Lin, A. Pozdnyakov, S.S. Yu

National Taiwan University (NTU), Taipei, Taiwan

P. Chang, Y. Chao, K.F. Chen, P.H. Chen, F. Fiori, W.-S. Hou, Y. Hsiung, Arun Kumar, Y.F. Liu, R.-S. Lu, E. Paganis, A. Psallidas, A. Steen, J.f. Tsai

Chulalongkorn University, Faculty of Science, Department of Physics, Bangkok, Thailand

B. Asavapibhop, K. Kovitangoon, G. Singh, N. Srimanobhas

Çukurova University, Physics Department, Science and Art Faculty, Adana, Turkey

A. Bat, F. Boran, S. Cerci⁴⁹, S. Damarseckin, Z.S. Demiroglu, C. Dozen, I. Dumanoglu, S. Girgis, G. Gokbulut, Y. Guler, I. Hos⁵⁰, E.E. Kanga⁵¹, O. Kara, A. Kayis Topaksu, U. Kiminsu, M. Oglakci, G. Onengut⁵², K. Ozdemir⁵³, D. Sunar Cerci⁴⁹, B. Tali⁴⁹, U.G. Tok, S. Turkcapar, I.S. Zorbakir, C. Zorbilmez

Middle East Technical University, Physics Department, Ankara, Turkey

B. Bilin, G. Karapinar⁵⁴, K. Ocalan⁵⁵, M. Yalvac, M. Zeyrek

Bogazici University, Istanbul, Turkey

E. Gülmez, M. Kaya⁵⁶, O. Kaya⁵⁷, S. Tekten, E.A. Yetkin⁵⁸

Istanbul Technical University, Istanbul, Turkey

M.N. Agaras, S. Atay, A. Cakir, K. Cankocak

Institute for Scintillation Materials of National Academy of Science of Ukraine, Kharkov, Ukraine

B. Grynyov

National Scientific Center, Kharkov Institute of Physics and Technology, Kharkov, Ukraine

L. Levchuk

University of Bristol, Bristol, United Kingdom

F. Ball, L. Beck, J.J. Brooke, D. Burns, E. Clement, D. Cussans, O. Davignon, H. Flacher, J. Goldstein, G.P. Heath, H.F. Heath, L. Kreczko, D.M. Newbold⁵⁹, S. Paramesvaran, T. Sakuma, S. Seif El Nasr-storey, D. Smith, V.J. Smith

Rutherford Appleton Laboratory, Didcot, United Kingdom

K.W. Bell, A. Belyaev⁶⁰, C. Brew, R.M. Brown, L. Calligaris, D. Cieri, D.J.A. Cockerill, J.A. Coughlan, K. Harder, S. Harper, E. Olaiya, D. Petyt, C.H. Shepherd-Themistocleous, A. Thea, I.R. Tomalin, T. Williams

Imperial College, London, United Kingdom

G. Auzinger, R. Bainbridge, J. Borg, S. Breeze, O. Buchmuller, A. Bundock, S. Casasso, M. Citron, D. Colling, L. Corpe, P. Dauncey, G. Davies, A. De Wit, M. Della Negra, R. Di Maria, A. Elwood, Y. Haddad, G. Hall, G. Iles, T. James, R. Lane, C. Laner, L. Lyons, A.-M. Magnan,

S. Malik, L. Mastrolorenzo, T. Matsushita, J. Nash, A. Nikitenko⁷, V. Palladino, M. Pesaresi, D.M. Raymond, A. Richards, A. Rose, E. Scott, C. Seez, A. Shtipliyski, S. Summers, A. Tapper, K. Uchida, M. Vazquez Acosta⁶¹, T. Virdee¹⁴, N. Wardle, D. Winterbottom, J. Wright, S.C. Zenz

Brunel University, Uxbridge, United Kingdom

J.E. Cole, P.R. Hobson, A. Khan, P. Kyberd, I.D. Reid, P. Symonds, L. Teodorescu, M. Turner, S. Zahid

Baylor University, Waco, USA

A. Borzou, K. Call, J. Dittmann, K. Hatakeyama, H. Liu, N. Pastika, C. Smith

Catholic University of America, Washington DC, USA

R. Bartek, A. Dominguez

The University of Alabama, Tuscaloosa, USA

A. Buccilli, S.I. Cooper, C. Henderson, P. Rumerio, C. West

Boston University, Boston, USA

D. Arcaro, A. Avetisyan, T. Bose, D. Gastler, D. Rankin, C. Richardson, J. Rohlf, L. Sulak, D. Zou

Brown University, Providence, USA

G. Benelli, D. Cutts, A. Garabedian, M. Hadley, J. Hakala, U. Heintz, J.M. Hogan, K.H.M. Kwok, E. Laird, G. Landsberg, J. Lee, Z. Mao, M. Narain, J. Pazzini, S. Piperov, S. Sagir, R. Syarif, D. Yu

University of California, Davis, Davis, USA

R. Band, C. Brainerd, R. Breedon, D. Burns, M. Calderon De La Barca Sanchez, M. Chertok, J. Conway, R. Conway, P.T. Cox, R. Erbacher, C. Flores, G. Funk, M. Gardner, W. Ko, R. Lander, C. Mclean, M. Mulhearn, D. Pellett, J. Pilot, S. Shalhout, M. Shi, J. Smith, D. Stolp, K. Tos, M. Tripathi, Z. Wang

University of California, Los Angeles, USA

M. Bachtis, C. Bravo, R. Cousins, A. Dasgupta, A. Florent, J. Hauser, M. Ignatenko, N. Mccoll, S. Regnard, D. Saltzberg, C. Schnaible, V. Valuev

University of California, Riverside, Riverside, USA

E. Bouvier, K. Burt, R. Clare, J. Ellison, J.W. Gary, S.M.A. Ghiasi Shirazi, G. Hanson, J. Heilman, E. Kennedy, F. Lacroix, O.R. Long, M. Olmedo Negrete, M.I. Paneva, W. Si, L. Wang, H. Wei, S. Wimpenny, B. R. Yates

University of California, San Diego, La Jolla, USA

J.G. Branson, S. Cittolin, M. Derdzinski, R. Gerosa, D. Gilbert, B. Hashemi, A. Holzner, D. Klein, G. Kole, V. Krutelyov, J. Letts, I. Macneill, M. Masciovecchio, D. Olivito, S. Padhi, M. Pieri, M. Sani, V. Sharma, S. Simon, M. Tadel, A. Vartak, S. Wasserbaech⁶², J. Wood, F. Würthwein, A. Yagil, G. Zevi Della Porta

University of California, Santa Barbara - Department of Physics, Santa Barbara, USA

N. Amin, R. Bhandari, J. Bradmiller-Feld, C. Campagnari, A. Dishaw, V. Dutta, M. Franco Sevilla, C. George, F. Golf, L. Gouskos, J. Gran, R. Heller, J. Incandela, A. Ovcharova, H. Qu, J. Richman, D. Stuart, I. Suarez, J. Yoo

California Institute of Technology, Pasadena, USA

D. Anderson, A. Bornheim, J.M. Lawhorn, H.B. Newman, T. Nguyen, C. Pena, M. Spiropulu, J.R. Vlimant, S. Xie, Z. Zhang, R.Y. Zhu

Carnegie Mellon University, Pittsburgh, USA

M.B. Andrews, T. Ferguson, T. Mudholkar, M. Paulini, J. Russ, M. Sun, H. Vogel, I. Vorobiev, M. Weinberg

University of Colorado Boulder, Boulder, USA

J.P. Cumalat, W.T. Ford, F. Jensen, A. Johnson, M. Krohn, S. Leontsinis, T. Mulholland, K. Stenson, S.R. Wagner

Cornell University, Ithaca, USA

J. Alexander, J. Chaves, J. Chu, S. Dittmer, K. Mcdermott, N. Mirman, J.R. Patterson, D. Quach, A. Rinkevicius, A. Ryd, L. Skinnari, L. Soffi, S.M. Tan, Z. Tao, J. Thom, J. Tucker, P. Wittich, M. Zientek

Fermi National Accelerator Laboratory, Batavia, USA

S. Abdullin, M. Albrow, M. Alyari, G. Apollinari, A. Apresyan, A. Apyan, S. Banerjee, L.A.T. Bauerdick, A. Beretvas, J. Berryhill, P.C. Bhat, G. Bolla[†], K. Burkett, J.N. Butler, A. Canepa, G.B. Cerati, H.W.K. Cheung, F. Chlebana, M. Cremonesi, J. Duarte, V.D. Elvira, J. Freeman, Z. Gecse, E. Gottschalk, L. Gray, D. Green, S. Grünendahl, O. Gutsche, R.M. Harris, S. Hasegawa, J. Hirschauer, Z. Hu, B. Jayatilaka, S. Jindariani, M. Johnson, U. Joshi, B. Klima, B. Kreis, S. Lammel, D. Lincoln, R. Lipton, M. Liu, T. Liu, R. Lopes De Sá, J. Lykken, K. Maeshima, N. Magini, J.M. Marraffino, D. Mason, P. McBride, P. Merkel, S. Mrenna, S. Nahn, V. O'Dell, K. Pedro, O. Prokofyev, G. Rakness, L. Ristori, B. Schneider, E. Sexton-Kennedy, A. Soha, W.J. Spalding, L. Spiegel, S. Stoynev, J. Strait, N. Strobbe, L. Taylor, S. Tkaczyk, N.V. Tran, L. Uplegger, E.W. Vaandering, C. Vernieri, M. Verzocchi, R. Vidal, M. Wang, H.A. Weber, A. Whitbeck

University of Florida, Gainesville, USA

D. Acosta, P. Avery, P. Bortignon, D. Bourilkov, A. Brinkerhoff, A. Carnes, M. Carver, D. Curry, R.D. Field, I.K. Furic, S.V. Gleyzer, B.M. Joshi, J. Konigsberg, A. Korytov, K. Kotov, P. Ma, K. Matchev, H. Mei, G. Mitselmakher, D. Rank, K. Shi, D. Sperka, N. Terentyev, L. Thomas, J. Wang, S. Wang, J. Yelton

Florida International University, Miami, USA

Y.R. Joshi, S. Linn, P. Markowitz, J.L. Rodriguez

Florida State University, Tallahassee, USA

A. Ackert, T. Adams, A. Askew, S. Hagopian, V. Hagopian, K.F. Johnson, T. Kolberg, G. Martinez, T. Perry, H. Prosper, A. Saha, A. Santra, V. Sharma, R. Yohay

Florida Institute of Technology, Melbourne, USA

M.M. Baarmand, V. Bhopatkar, S. Colafranceschi, M. Hohlmann, D. Noonan, T. Roy, F. Yumiceva

University of Illinois at Chicago (UIC), Chicago, USA

M.R. Adams, L. Apanasevich, D. Berry, R.R. Betts, R. Cavanaugh, X. Chen, O. Evdokimov, C.E. Gerber, D.A. Hangal, D.J. Hofman, K. Jung, J. Kamin, I.D. Sandoval Gonzalez, M.B. Tonjes, H. Trauger, N. Varelas, H. Wang, Z. Wu, J. Zhang

The University of Iowa, Iowa City, USA

B. Bilki⁶³, W. Clarida, K. Dilsiz⁶⁴, S. Durgut, R.P. Gandrajula, M. Haytmyradov, V. Khristenko, J.-P. Merlo, H. Mermerkaya⁶⁵, A. Mestvirishvili, A. Moeller, J. Nachtman, H. Ogul⁶⁶, Y. Onel, F. Ozok⁶⁷, A. Penzo, C. Snyder, E. Tiras, J. Wetzel, K. Yi

Johns Hopkins University, Baltimore, USA

B. Blumenfeld, A. Cocoros, N. Eminizer, D. Fehling, L. Feng, A.V. Gritsan, P. Maksimovic, J. Roskes, U. Sarica, M. Swartz, M. Xiao, C. You

The University of Kansas, Lawrence, USA

A. Al-bataineh, P. Baringer, A. Bean, S. Boren, J. Bowen, J. Castle, S. Khalil, A. Kropivnitskaya, D. Majumder, W. Mcbrayer, M. Murray, C. Royon, S. Sanders, E. Schmitz, J.D. Tapia Takaki, Q. Wang

Kansas State University, Manhattan, USA

A. Ivanov, K. Kaadze, Y. Maravin, A. Mohammadi, L.K. Saini, N. Skhirtladze, S. Toda

Lawrence Livermore National Laboratory, Livermore, USA

F. Rebassoo, D. Wright

University of Maryland, College Park, USA

C. Anelli, A. Baden, O. Baron, A. Belloni, B. Calvert, S.C. Eno, Y. Feng, C. Ferraioli, N.J. Hadley, S. Jabeen, G.Y. Jeng, R.G. Kellogg, J. Kunkle, A.C. Mignerey, F. Ricci-Tam, Y.H. Shin, A. Skuja, S.C. Tonwar

Massachusetts Institute of Technology, Cambridge, USA

D. Abercrombie, B. Allen, V. Azzolini, R. Barbieri, A. Baty, R. Bi, S. Brandt, W. Busza, I.A. Cali, M. D'Alfonso, Z. Demiragli, G. Gomez Ceballos, M. Goncharov, D. Hsu, M. Hu, Y. Iiyama, G.M. Innocenti, M. Klute, D. Kovalskyi, Y.S. Lai, Y.-J. Lee, A. Levin, P.D. Luckey, B. Maier, A.C. Marini, C. Mcginn, C. Mironov, S. Narayanan, X. Niu, C. Paus, C. Roland, G. Roland, J. Salfeld-Nebgen, G.S.F. Stephans, K. Tatar, D. Velicanu, J. Wang, T.W. Wang, B. Wyslouch

University of Minnesota, Minneapolis, USA

A.C. Benvenuti, R.M. Chatterjee, A. Evans, P. Hansen, J. Hiltbrand, S. Kalafut, Y. Kubota, Z. Lesko, J. Mans, S. Nourbakhsh, N. Ruckstuhl, R. Rusack, J. Turkewitz, M.A. Wadud

University of Mississippi, Oxford, USA

J.G. Acosta, S. Oliveros

University of Nebraska-Lincoln, Lincoln, USA

E. Avdeeva, K. Bloom, D.R. Claes, C. Fangmeier, R. Gonzalez Suarez, R. Kamalieddin, I. Kravchenko, J. Monroy, J.E. Siado, G.R. Snow, B. Stieger

State University of New York at Buffalo, Buffalo, USA

J. Dolen, A. Godshalk, C. Harrington, I. Iashvili, D. Nguyen, A. Parker, S. Rappoccio, B. Roozbahani

Northeastern University, Boston, USA

G. Alverson, E. Barberis, A. Hortiangtham, A. Massironi, D.M. Morse, T. Orimoto, R. Teixeira De Lima, D. Trocino, D. Wood

Northwestern University, Evanston, USA

S. Bhattacharya, O. Charaf, K.A. Hahn, N. Mucia, N. Odell, B. Pollack, M.H. Schmitt, K. Sung, M. Trovato, M. Velasco

University of Notre Dame, Notre Dame, USA

N. Dev, M. Hildreth, K. Hurtado Anampa, C. Jessop, D.J. Karmgard, N. Kellams, K. Lannon, N. Loukas, N. Marinelli, F. Meng, C. Mueller, Y. Musienko³⁵, M. Planer, A. Reinsvold, R. Ruchti, G. Smith, S. Taroni, M. Wayne, M. Wolf, A. Woodard

The Ohio State University, Columbus, USA

J. Alimena, L. Antonelli, B. Bylsma, L.S. Durkin, S. Flowers, B. Francis, A. Hart, C. Hill, W. Ji, B. Liu, W. Luo, B.L. Winer, H.W. Wulsin

Princeton University, Princeton, USA

S. Cooperstein, O. Driga, P. Elmer, J. Hardenbrook, P. Hebda, S. Higginbotham, D. Lange, J. Luo, D. Marlow, K. Mei, I. Ojalvo, J. Olsen, C. Palmer, P. Piroué, D. Stickland, C. Tully

University of Puerto Rico, Mayaguez, USA

S. Malik, S. Norberg

Purdue University, West Lafayette, USA

A. Barker, V.E. Barnes, S. Das, S. Folgueras, L. Gutay, M.K. Jha, M. Jones, A.W. Jung, A. Khatiwada, D.H. Miller, N. Neumeister, C.C. Peng, H. Qiu, J.F. Schulte, J. Sun, F. Wang, W. Xie

Purdue University Northwest, Hammond, USA

T. Cheng, N. Parashar, J. Stupak

Rice University, Houston, USA

A. Adair, Z. Chen, K.M. Ecklund, S. Freed, F.J.M. Geurts, M. Guilbaud, M. Kilpatrick, W. Li, B. Michlin, M. Northup, B.P. Padley, J. Roberts, J. Rorie, W. Shi, Z. Tu, J. Zabel, A. Zhang

University of Rochester, Rochester, USA

A. Bodek, P. de Barbaro, R. Demina, Y.t. Duh, T. Ferbel, M. Galanti, A. Garcia-Bellido, J. Han, O. Hindrichs, A. Khukhunaishvili, K.H. Lo, P. Tan, M. Verzetti

The Rockefeller University, New York, USA

R. Ciesielski, K. Goulianos, C. Mesropian

Rutgers, The State University of New Jersey, Piscataway, USA

A. Agapitos, J.P. Chou, Y. Gershtein, T.A. Gómez Espinosa, E. Halkiadakis, M. Heindl, E. Hughes, S. Kaplan, R. Kunnawalkam Elayavalli, S. Kyriacou, A. Lath, R. Montalvo, K. Nash, M. Osherson, H. Saka, S. Salur, S. Schnetzer, D. Sheffield, S. Somalwar, R. Stone, S. Thomas, P. Thomassen, M. Walker

University of Tennessee, Knoxville, USA

A.G. Delannoy, M. Foerster, J. Heideman, G. Riley, K. Rose, S. Spanier, K. Thapa

Texas A&M University, College Station, USA

O. Bouhali⁶⁸, A. Castaneda Hernandez⁶⁸, A. Celik, M. Dalchenko, M. De Mattia, A. Delgado, S. Dildick, R. Eusebi, J. Gilmore, T. Huang, T. Kamon⁶⁹, R. Mueller, Y. Pakhotin, R. Patel, A. Perloff, L. Perniè, D. Rathjens, A. Safonov, A. Tatarinov, K.A. Ulmer

Texas Tech University, Lubbock, USA

N. Akchurin, J. Damgov, F. De Guio, P.R. Duderod, J. Faulkner, E. Gurpinar, S. Kunori, K. Lamichhane, S.W. Lee, T. Libeiro, T. Mengke, S. Muthumuni, T. Peltola, S. Undleeb, I. Volobouev, Z. Wang

Vanderbilt University, Nashville, USA

S. Greene, A. Gurrola, R. Janjam, W. Johns, C. Maguire, A. Melo, H. Ni, K. Padeken, P. Sheldon, S. Tuo, J. Velkovska, Q. Xu

University of Virginia, Charlottesville, USA

M.W. Arenton, P. Barria, B. Cox, R. Hirosky, M. Joyce, A. Ledovskoy, H. Li, C. Neu, T. Sinthuprasith, Y. Wang, E. Wolfe, F. Xia

Wayne State University, Detroit, USA

R. Harr, P.E. Karchin, N. Poudyal, J. Sturdy, P. Thapa, S. Zaleski

University of Wisconsin - Madison, Madison, WI, USA

M. Brodski, J. Buchanan, C. Caillol, S. Dasu, L. Dodd, S. Duric, B. Gomber, M. Grothe, M. Herndon, A. Hervé, U. Hussain, P. Klabbers, A. Lanaro, A. Levine, K. Long, R. Loveless, G. Polese, T. Ruggles, A. Savin, N. Smith, W.H. Smith, D. Taylor, N. Woods

†: Deceased

1: Also at Vienna University of Technology, Vienna, Austria

2: Also at State Key Laboratory of Nuclear Physics and Technology; Peking University, Beijing, China

3: Also at IRFU; CEA; Université Paris-Saclay, Gif-sur-Yvette, France

4: Also at Universidade Estadual de Campinas, Campinas, Brazil

5: Also at Universidade Federal de Pelotas, Pelotas, Brazil

6: Also at Université Libre de Bruxelles, Bruxelles, Belgium

7: Also at Institute for Theoretical and Experimental Physics, Moscow, Russia

8: Also at Joint Institute for Nuclear Research, Dubna, Russia

9: Now at Ain Shams University, Cairo, Egypt

10: Now at British University in Egypt, Cairo, Egypt

11: Also at Zewail City of Science and Technology, Zewail, Egypt

12: Also at Université de Haute Alsace, Mulhouse, France

13: Also at Skobeltsyn Institute of Nuclear Physics; Lomonosov Moscow State University, Moscow, Russia

14: Also at CERN; European Organization for Nuclear Research, Geneva, Switzerland

15: Also at RWTH Aachen University; III. Physikalisches Institut A, Aachen, Germany

16: Also at University of Hamburg, Hamburg, Germany

17: Also at Brandenburg University of Technology, Cottbus, Germany

18: Also at MTA-ELTE Lendület CMS Particle and Nuclear Physics Group; Eötvös Loránd University, Budapest, Hungary

19: Also at Institute of Nuclear Research ATOMKI, Debrecen, Hungary

20: Also at Institute of Physics; University of Debrecen, Debrecen, Hungary

21: Also at Indian Institute of Technology Bhubaneswar, Bhubaneswar, India

22: Also at Institute of Physics, Bhubaneswar, India

23: Also at University of Visva-Bharati, Santiniketan, India

24: Also at University of Ruhuna, Matara, Sri Lanka

25: Also at Isfahan University of Technology, Isfahan, Iran

26: Also at Yazd University, Yazd, Iran

27: Also at Plasma Physics Research Center; Science and Research Branch; Islamic Azad University, Tehran, Iran

28: Also at Università degli Studi di Siena, Siena, Italy

29: Also at INFN Sezione di Milano-Bicocca; Università di Milano-Bicocca, Milano, Italy

30: Also at Purdue University, West Lafayette, USA

31: Also at International Islamic University of Malaysia, Kuala Lumpur, Malaysia

32: Also at Malaysian Nuclear Agency; MOSTI, Kajang, Malaysia

33: Also at Consejo Nacional de Ciencia y Tecnología, Mexico city, Mexico

34: Also at Warsaw University of Technology; Institute of Electronic Systems, Warsaw, Poland

35: Also at Institute for Nuclear Research, Moscow, Russia

36: Now at National Research Nuclear University 'Moscow Engineering Physics Institute' (MEPhI), Moscow, Russia

- 37: Also at St. Petersburg State Polytechnical University, St. Petersburg, Russia
- 38: Also at University of Florida, Gainesville, USA
- 39: Also at P.N. Lebedev Physical Institute, Moscow, Russia
- 40: Also at California Institute of Technology, Pasadena, USA
- 41: Also at Budker Institute of Nuclear Physics, Novosibirsk, Russia
- 42: Also at Faculty of Physics; University of Belgrade, Belgrade, Serbia
- 43: Also at University of Belgrade; Faculty of Physics and Vinca Institute of Nuclear Sciences, Belgrade, Serbia
- 44: Also at Scuola Normale e Sezione dell'INFN, Pisa, Italy
- 45: Also at National and Kapodistrian University of Athens, Athens, Greece
- 46: Also at Riga Technical University, Riga, Latvia
- 47: Also at Universität Zürich, Zurich, Switzerland
- 48: Also at Stefan Meyer Institute for Subatomic Physics (SMI), Vienna, Austria
- 49: Also at Adiyaman University, Adiyaman, Turkey
- 50: Also at Istanbul Aydin University, Istanbul, Turkey
- 51: Also at Mersin University, Mersin, Turkey
- 52: Also at Cag University, Mersin, Turkey
- 53: Also at Piri Reis University, Istanbul, Turkey
- 54: Also at Izmir Institute of Technology, Izmir, Turkey
- 55: Also at Necmettin Erbakan University, Konya, Turkey
- 56: Also at Marmara University, Istanbul, Turkey
- 57: Also at Kafkas University, Kars, Turkey
- 58: Also at Istanbul Bilgi University, Istanbul, Turkey
- 59: Also at Rutherford Appleton Laboratory, Didcot, United Kingdom
- 60: Also at School of Physics and Astronomy; University of Southampton, Southampton, United Kingdom
- 61: Also at Instituto de Astrofísica de Canarias, La Laguna, Spain
- 62: Also at Utah Valley University, Orem, USA
- 63: Also at Beykent University, Istanbul, Turkey
- 64: Also at Bingol University, Bingol, Turkey
- 65: Also at Erzincan University, Erzincan, Turkey
- 66: Also at Sinop University, Sinop, Turkey
- 67: Also at Mimar Sinan University; Istanbul, Istanbul, Turkey
- 68: Also at Texas A&M University at Qatar, Doha, Qatar
- 69: Also at Kyungpook National University, Daegu, Korea